**Table 3 Fitted initial (t = 0) values for the *in vitro* experiment**

| Variable | Unit | Fitted initial value at MOI of | | | |
|---|---|---|---|---|---|
| | | $2 \times 10^{-3}$ | $2 \times 10^{-4}$ | $2 \times 10^{-5}$ | $2 \times 10^{-6}$ |
| $x_j(0)$ | cells/ml | $6.55 \times 10^6$ | $6.50 \times 10^6$ | $5.82 \times 10^6$ | $4.94 \times 10^6$ |
| $y_j(0)$ | cells/ml | $6.47 \times 10^2$ | $1.60 \times 10^2$ | $6.89 \times 10^{-3}$ | 0.254 |
| $v_{RNAj}(0)$ | RNA copies/ml | $9.15 \times 10^6$ | $1.05 \times 10^6$ | $1.58 \times 10^5$ | $8.21 \times 10^3$ |
| $v_{50j}(0)$ | $TCID_{50}$/ml | 43.1 | 0.162 | 2.92 | 2.99 |

negative and Nef-positive HSC-F cells [cells/ml], the total SHIV-KS661 viral load [RNA copies/ml], and the infectious viral load [$TCID_{50}$/ml]. At each daily measurement, almost all of the culture supernatant (99.93%) was removed for viral counting; a small percentage of cells (5.5%) were removed for counting and FACS analysis, and the remaining cells were thoroughly washed and replaced in fresh medium. The experiment was repeated for four different values of the initial viral inoculum (MOI). In total, we obtained 130 data points for quantifying SHIV-KS661 viral kinetics *in vitro* (Table 1 **and** Figure 3).

In examining the MOI = $2 \times 10^{-3}$ data, one can see that the target cell population remains high (near its initial value of approximately $6.46 \times 10^6$ cells/ml) until just before the peak of the virus concentration, at which point the target cell population decreases rapidly. The total infected cell population, the total virus count (RNA/ml), and the infectious virus count ($TCID_{50}$/ml) all peak around $t = 3$ days. Moreover, the rate of exponential decay (downward slope) of the total virus and the infected cell population after their respective peaks are quite similar. This behavior is expected: since the virus is being almost completely removed from the culture on a daily basis due to sampling and the RNA degradation rate is very small ($r_{RNA} = 0.039$ per day); the measured RNA count of virus is nearly equal to the total number of virus produced over the preceding day which should be proportional to the number of cells producing virus. Similar reasoning should apply to the decay of infectious virus - the net infectious virus measured after one day should also be approximately proportional to the number of infected cells - but the rates appear much less closely aligned in this case, perhaps due to larger errors in the $TCID_{50}$ measurement technique. Alternatively, the observed more rapid than expected decrease of infectious virus could have a biological cause. For instance, the co-infection of cells by competent and defective interfering viruses at late stages in the experiment could lead to an enhanced production of the latter [40], thus successively reducing the fraction of infectious particles. An increase in cell-death by-products could also contribute to the decline in virus infectivity. In SIV and SHIV infections *in vivo*, a decreasing viral infectiousness has been observed over time

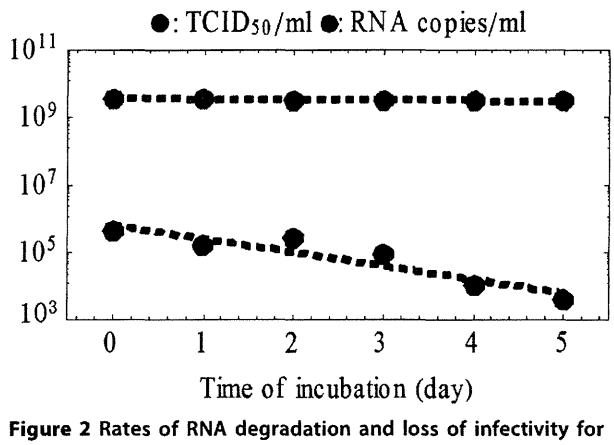


**Figure 2 Rates of RNA degradation and loss of infectivity for SHIV-KS661**. Stock virus was incubated under the same conditions as the infection experiments, but in the absence of cells, then sampled every day and stored at -80°C. After the sampling, the RNA copy number (gray circles) and 50% tissue culture infectious dose (black circles) of the samples were measured. Linear regressions yielded a rate of RNA degradation of $r_{RNA} = 0.039$ per day and a rate of loss of viral infectivity of $r_I = 0.93$ per day.

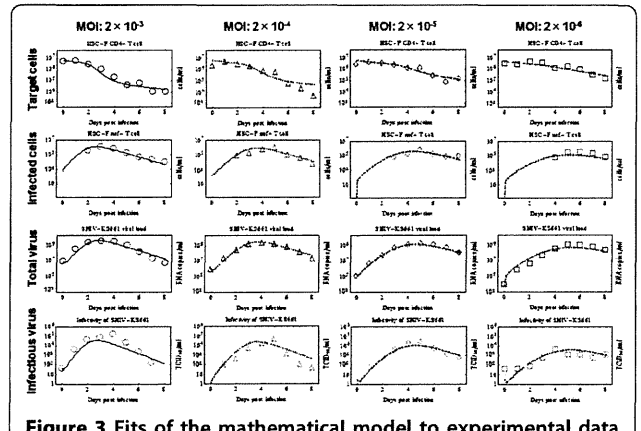


**Figure 3 Fits of the mathematical model to experimental data of SHIV-KS661 *in vitro***. HSC-F cells were inoculated with SHIV-KS661 24 h before $t = 0$, and each *in vitro* experimental quantity was measured daily from $t = 0$ d to 8 d. The curves show the best-fit of the model (Eqs.(5)-(8), lines) to the experimental data (points) for the target cells, infected cells, and the total and infectious viral load for the four different experiments conducted at different MOIs. All data were fitted simultaneously as described in the text. The fitted $t = 0$ values of each quantity are given in **Table 3**.

[7,41,42], but the timescale of this decay is longer than that observed here and likely has an in-host origin.

A comparison of the experiments at the four different MOI values shows that a decrease in the initial viral inoculum serves primarily to delay the course of the infection. The target cell populations drop to approximately half of their original values at $t \approx 1.9, 2.6, 3.5$ and $4.1$ days, respectively, for the four experiments in order of decreasing MOI. Similarly the peaks of the total viral RNA occur at $t \approx 3.0, 4.0, 5.0$ and $5.5$ days, respectively. The experiments at lower MOI have slightly lower viral and infected cell peaks, but differ from those of the experiment at MOI = $2 \times 10^{-3}$ by less than a factor of three.

### Relevant SHIV-KS661 viral kinetics measures

Having fixed the values of the rates of virion decay ($r_I$ and $r_{RNA}$) and the target cell death rate ($d$) using separate experiments, we estimated the values and 95% CI of the four remaining unknown parameters ($\beta_{50}$, $a$, $k$, $k_{50}$) by fitting the model in Eqs.(5)-(8) to the full *in vitro* dataset simultaneously (Table 2). The death rate of infected cells was determined to be $a = 1.18$ per day (95%CI: *0.85-1.26* per day) which implies that the half-life of infected cells (i.e., $log2/a$) is *14.1* h. Infected HSC-F cells were found to produce $k = 2.61 \times 10^4$ RNA copies of virus per day.

From the directly fitted parameters, we also calculated a number of important derived quantities and their 95% CI, determined from the bootstrap fits (Table 2). One key measurement of viral kinetics is the viral burst size, which is the total number of virus produced by an infected cell during its lifetime [18-20]. The total burst size of SHIV-KS661 (including non-infectious and infectious virus) is given in our model by $k/a$ and was estimated from our *in vitro* experiment to be $2.21 \times 10^4$ RNA copies. The burst size of infectious SHIV-KS661, $k_{50}/a$, was *0.19* $TCID_{50}$.

To broadly characterize viral kinetics, it is instructive to calculate the basic reproductive number for the system, which has the form $R_0 = \beta_{50}k_{50}x_0/(a(r_I+r_{RNA}))$ and is interpreted as the number of newly infected cells intrinsically generated by a single infectious cell at the start of the infection [15-19,27]. The initial number of HSC-F cells, $x_0$, was approximately $6.46 \times 10^6$ cells/ml, which, together with the values of the five estimated parameters, yields an estimate for the basic reproductive number of *62.8*. This large value ($62.8 \gg 1$) implies that, given a small initiating infected cell population, the infection is overwhelmingly likely to spread to the entire population of cells.

After the repetitive removal of cells and virus begins, the basic reproductive number is effectively reduced, much like the effect of quarantine on the epidemiological measure of $R_0$. When the effects of removal are included in the calculation of the basic reproductive number it has the form $R_0^* = \beta_{50}k_{50}x_0/((a+\delta)(r_I+r_{RNA}+r_C))$ which yields a smaller value of 7.01. This value better characterizes the course of the infection in our system, for example, through the recursive relation for the approximate fraction of eventually infected cells, $f_I = 1- exp(-R_0^* f_I)$ [43]. Using this expression, we find that the fraction of target cells at the end of the infection ($1-f_I$) should be $9.01 \times 10^{-4}$, which implies an approximately final target cell concentration is $5.87 \times 10^3$ cells/ml. This value agrees well with the asymptotic concentration of Nef-negative HSC-F cells in the MOI = $2 \times 10^{-3}$ experiment, $\sim 1.03 \times 10^4$ cells/ml. The delay of the infection precludes an estimate of the final target cell value at smaller MOI values.

Our model formulation also enables us to determine, albiet not fully, two interesting quantities related to the infectiousness of SHIV-KS66 virions. Parameter $p$ (where $0 < p \leqq 1$) is the fraction of SHIV-KS66 virions which are infectious at the time of production: the larger the value of $p$, the fewer defective virus particles are produced by infectious cells. Parameter $\alpha$ is approximately the fraction of infectious virions which are measured in the $TCID_{50}$ assay, i.e., it is the ratio of $TCID_{50}$ viral titer ($v_{50}$) to the RNA count of infectious virions ($v_I$). It follows from Poisson statistics that $0 < \alpha \leqq 1.47$ $TCID_{50}$ per infectious RNA copies of infectious virions. While we cannot determine $p$ and $\alpha$ individually in our analysis, their product is given by $k_{50}/k = (\alpha pk)/k = \alpha p = 8.63 \times 10^{-6}$ $TCID_{50}$ per infectious RNA copies. Because of the upper bounds on $p$ and $\alpha$, the value of their product imposes a minimum condition on each: $5.87 \times 10^{-6} < p \leqq 1$ and $8.63 \times 10^{-6} < \alpha \leqq 1.47$ $TCID_{50}$ per RNA copies.

We can constrain these parameters further by considering the basic reproductive number $R_0 = 62.8$, which implies that one infectious cell will infect *62.8* other cells over the course of its infectious lifespan. Thus, one infectious cell must produce at least *62.8* infectious virions over its lifespan, i.e., have a burst size of at least *62.8* infectious RNA copies. The burst size in infectious virions is given by $pk/a$, so this requirement can be written as $pk/a \geq R_0$ infectious RNA copies (or, equivalently, $p \geq aR_0/k$ infectious RNA copies) which, based on the values of these quantities from Table 2 implies that $p \geq 2.84 \times 10^{-3}$. Thus $2.84 \times 10^{-3} \leqq p \leqq 1$, which means that at least one in every 350 virions produced is infectious. Since $\alpha p = 8.63 \times 10^{-6}$ $TCID_{50}$ per infectious RNA copies, it follows that $8.63 \times 10^{-6} < \alpha \leqq 3.04 \times 10^{-3}$ $TCID_{50}$ per infectious RNA copies, which means that 1 $TCID_{50}$ corresponds to at least *330* ($1/3.04 \times 10^{-3}$) infectious virus, but perhaps as many as *120, 000* ($1/8.63 \times 10^{-6}$).

## Discussion

We have applied a simple mathematical model to quantitatively characterize the *in vitro* kinetics of SHIV-KS661 virus infection in HSC-F cell cultures, leveraging experimental data for total and infectious viral load, along with target and infected cell dynamics, to fully parameterize the system. Specifically, we determined values for the rate of loss of infectivity and the RNA degradation rate of SHIV-KS661, the target and infected HSC-F cell half-life, the rate constant for infection of target cells and the infectious and total viral production rates of infected cells. From these fundamental quantities, we also estimated a number of important derived quantities, including the burst size of an infected cell and the basic reproductive number. Additionally, by measuring both the total and infectious viral load within the context of a mathematical model we were able to provide a lower bound for the proportion of infectious virions produced by infected cells.

We estimated the half-life of SHIV-infected HSC-F cells to be *14.1* h. In clinical studies of patients or animals, it is extremely difficult to continuously measure the number of infected cells during infection. This is because the amount of infected cells in peripheral blood (PB) is very small. For example, in HIV-1 infected patients, there are only about $10^2$ infected cells per $10^6$ peripheral blood mononuclear cells at their set point [14]. Thus, measuring the number of infected cells in PB during the early phase of infection is technically difficult. In HIV-1 humanized mice, infected cells in PB are not detectable even during the acute phase when 80-90% of target cells in the spleen and lymph nodes are infected (K. Sato and S. Iwami, unpublished data). For this reason, the death rate of infected cells *in vivo* has primarily been estimated from the viral load decay (or the decay of infectious virus) after the peak of an acute infection [11,16,17,20,27] or after antiviral drug administration [10,14,15,22]. The maximum half-lives of HIV-1 and SIV-infected cells were both initially estimated - by analysis of *in vivo* viral decay under antiviral therapy - to be ~24 h [14,27], but drug combinations with higher efficacy have reduced the estimates to ~17 and ~11 h, respectively [12,22,44]. Our *in vitro* estimate of the half-life, based on direct observations of Nef-positive cell decay, agrees well with these indirect *in vivo* measures, despite the absence of immune effects.

We determined an SHIV-KS661 viral burst size of $2.21 \times 10^4$ RNA or *0.19* $TCID_{50}$ for HSC-F cells. Current estimates of viral burst size in the literature rely on inhibiting multiple rounds of infection by antiviral drugs, washouts of infected cells, serial dilutions of infected cells, or infection by single-cycle virus [11,20,21,45,46]. The inhibition of the multiple rounds of infection, however, can introduce additional confounding factors on the viral burst size as discussed in [20]. Here, we have calculated the burst size of SHIV-KS661 in HSC-F cells indirectly by estimating the viral production rate and the average lifespan of infected cells over the course of a typical infection. Our estimate is quite close to the $\sim 5 \times 10^4$ RNA value determined in recent SIV single-cycle virion experiments *in vivo* [20], which, notably, was 10-100 times higher than most previously measured values. We also calculated a basic reproductive number for SHIV-KS661 in HSC-F cell cultures as approximately *62.8* for the initial stages of the infection and approximately *7.01* for the entire course, when the effects of manual removal of virus and cells are included. The latter value implies that reducing viral growth by about 85.7% for the entire course with antiviral intervention, for example, would prevent viral spread *in vitro* given the daily sampling.

It is widely believed that retroviruses are predominantly defective, with less than 0.1% of virions in plasma or culture media being infectious [47-49]. On the other hand, it has recently been suggested that HIV-1 virions, for example, are inherently highly infectious, but that slow viral diffusion in liquid media and rapid dissociation of virions from cells severely limit infections in cultures (i.e., in assays measuring infectivity) [50,51]. On both sides of this debate, however, studies have often relied on measurements of the proportion of infectious virus in stock samples, or on measurements of the infectious/non-infectious ratio over the course of an *in vitro* experiment. These direct measurements of the infectivity ratio in a virus sample are necessarily confounded by a continuous loss of infectious virus, driven by thermal deactivation and RNA degradation and, as such, these analyses cannot address the question of what fraction of virus are infectious at the time of production. Here, we have estimated the production rates of both infectious and non-infectious virus, allowing for a novel quantitative specification of the fraction of newly generated virus that is infectious. This fundamental quantity is important in understanding the role and influence of defective virus particles [48-50,52]; and, to our knowledge, this has not been measured before for any virus strain. We determined the theoretical minimum value for the proportion of infectious virions among newly produced virus, $p$, to be $8.62 \times 10^{-6}$, by calculating the ratio of the infectious to total viral production rates $k_{50}/k$. The ratio of the production rates, however, is actually $p$ multiplied by $\alpha$, where $\alpha$ is the conversion factor from RNA count of infectious virions to $TCID_{50}$ (i.e., roughly the fraction of infectious virions that are actually measured in a $TCID_{50}$ titration assay). Therefore, since $\alpha$ is likely much less than one, the proportion of infectious virus is likely much higher. In fact, using the

measured basic reproductive number, we estimate that the minimum value of $p$ is approximately $2.84 \times 10^{-3}$, meaning that at least 1 of every 350 virions produced is infectious. Determining this quantity is particularly important in determining the true efficiency of infectious virus replication. In previous publications [53,54], it was reported that *vif*-deficient HIV-1 showed decreased production of infectious virus due to the inhibition of the viral replication process by host factors such as APOBEC3 protein. Our method suggests a novel and more reliable way to determine the effect of the host-viral protein interaction on infectious viral replication.

In another aspect of viral infectivity, we found that the SHIV-KS661 virion infectious half-life at 37°C was 17.9 h. While this quantity is vital for understanding viral dynamics *in vitro*, and represents an important, strain-specific physical property of the virion, it is unlikely to strongly influence *in vivo* dynamics, due to the extremely high physical clearance rate in the blood (virion half-lives are on the order of minutes) [23].

## Conclusions

To conclude, by using a simple mathematical model for SHIV-KS661 infection on HSC-F cells and an abundant, diverse experimental dataset, we have been able to reliably estimate the parameters characterizing cell-virus interactions *in vitro*. Based on these estimated parameters, we have provided a quantitative description of SHIV-KS661 kinetics in HSC-F cell cultures which is consistent with previous studies of lentiviruses and provides a number of novel quantities. Most notably, our analysis provides an estimate of the minimum fraction of infectious virus produced by an infected cell. Our improved method for quantifying viral kinetics *in vitro* - which depends crucially on detailed time-course information about the infection of cells in addition to that of virus (both total particle count and infectious titer) - could be applied to other viral infections. The method could likely improve the understanding of the differences in replication across different strains [25,55] or between complete and protein-deficient viruses [53,54]; the differences in viral pathogenesis [6]; and the effects of anti-viral therapies [9,13]. Quantifying the *in vitro* viral kinetics for viruses such as HCV [56,57], for which a convenient animal experimental model has not been established, is of particular interest. Since the method presented here allows for the complete resolution of all viral kinetic parameters, it also enables the identification of the mechanisms of action for new antiviral compounds. Indeed, repeating the experimental infection under various antiviral concentrations would distinctly reveal which parameters (e.g., half-life of infected cells, infectious viral burst size) are affected by the antiviral and to what extent. Furthermore, the inhibitory concentration of the compound could be independently determined for each parameter. Thus, our synergistic approach, combining experiments and mathematical models, has broad potential applications in virology.

## Methods

### Virus and cell culture

The virus stock of SHIV-KS661 [5] was prepared in a $CD4^+$ human T lymphoid cell line, M8166 (a subclone of C8166) [58]. The stock was stored in liquid nitrogen until use. Establishment of the HSC-F cell line has been previously described [59]. This is a cynomolgous monkey $CD4^+$ T-cell line from fetal splenocytes that were immortalized by infection with Herpesvirus saimiri subtype C. The cells were cultured in RPMI-1640 medium supplemented with 10% fetal calf serum at 37°C and 5% $CO_2$ in humidified condition.

### *In vitro* experiment

Each experiment was performed using 2 wells of a 24-well plate with a total suspension volume of 2 ml (1 ml per well) and an initial cell concentration of $6.46 \times 10^6$ cells/ml in each well. Because the initial cell concentration is close to the carrying capacity of 24-well plates and the doubling time of HSC-F cells is not short, the population of target cells, in the absence of SHIV-KS661 infection, changes very little on the timescale of our experiment. We therefore neglected the effects of potential regeneration of HSC-F cells when constructing the mathematical model.

Cultures of HSC-F cells were inoculated at different MOIs ($2.0 \times 10^{-3}$, $2.0 \times 10^{-4}$, $2.0 \times 10^{-5}$, $2.0 \times 10^{-6}$; MOI = TCID50/cell) of SHIV-KS661 and incubated for 4 h at 37°C. After inoculation, cells were washed three times to remove the infection medium and placed in fresh media. Subsequently, the culture supernatant was harvested daily for 9 d, along with a small fraction of the cells (5.5%) for counting of viable and infected cells. The remaining cells were then gently washed three times and placed in a fresh, virus-free, medium. Separate experiments (not shown) determined that free virus was not completely removed, but that virus concentration in the supernatant dropped to 0.066% of its value prior to this sampling and washing procedure. Harvested culture supernatants were frozen and stored at -80°C until they were assayed via RT-PCR and $TCID_{50}$ titration, as described below.

### Count of viable and infected cells

Virus infection of the HSC-F cells was measured by FACS analysis using markers for intracellular SIV Nef antigen expression. The counts of total and viable cells were first determined using a cell counting chamber

(Burker-turk, Erma, Tokyo, Japan) with trypan blue staining. Viable HSC-F cells (gated by forward- and side-scatter results) were examined by flow cytometry to measure the intracellular SIV Nef antigen expression (see Figure 4). Cells were permeabilized with detergent-containing buffer (Permeabilizing Solution 2, BD Biosciences, San Jose, CA). The permeabilized cells were stained with anti-SIV Nef monoclonal antibody (04-001, Santa Cruz Biotechnology, Santa Cruz, CA) labeled by Zenon Alexa Fluor 488 (Invitrogen, Carlsbad, CA), and analyzed on FACSCalibur (BD Biosciences, San Jose, CA).

### Total and infectious viral load quantification

We followed the kinetics of both the total and infectious SHIV-KS661 viral load. The total viral load was measured with a real-time PCR quantification assay, as described previously [5], with minor modifications. Briefly, total RNA was isolated from the culture supernatants (140 μl) of virus-infected HSC-F cells with a QIAamp Viral RNA Mini kit (QIAGEN, Hilden, Germany). RT reactions and PCR were performed by a QuantiTect probe RT-PCR Kit (QIAGEN, Hilden, Germany) using the following primers for the *gag* region; SIV2-696F (5'-GGA AAT TAC CCA GTA CAA CAA ATAGG-3') and SIV2-784R (5'-TCT ATC AAT TTT ACC CAGGCA TTT A-3'). A labeled probe, SIV2-731T (5'-Fam-TGTCCA CCT GCC ATT AAG CCC G-Tamra-3'), was used for detection of the PCR products. These reactions were performed with a Prism 7500 Sequence Detector (Applied Biosystems, Foster City, CA) and analyzed using the manufacturer's software. For each run, a standard curve was generated from dilutions whose copy numbers were known, and the RNA in the culture supernatant samples was quantified based on the standard curve. The infectious viral load was measured by $TCID_{50}$ assay in HFC-S cell cultures using 96-well flat bottom plates at cell concentrations of $1.0 \times 10^6$ cells/ml. The titer of the virus was determined as described by Reed and Muench [60].

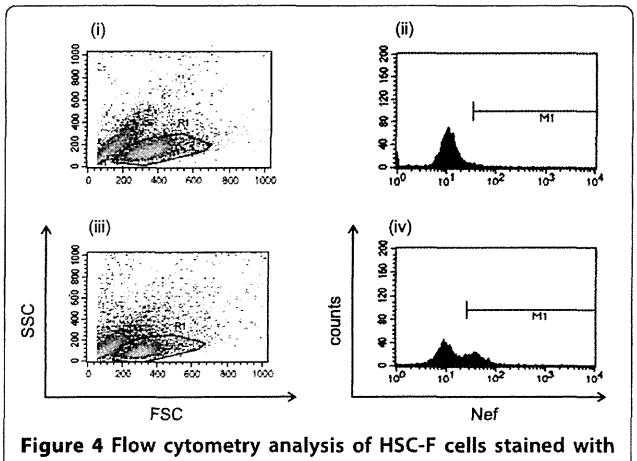


**Figure 4 Flow cytometry analysis of HSC-F cells stained with Nef antigen.** Representative data at 1 day (i and ii) and 5 days (iii and iv) post-inoculation with SHIV-KS661 at an MOI of $2 \times 10^{-5}$ are shown. The viable cell population, gated by the data of forward (FSC) and side scatter (SSC) (region surrounded with a solid line in (i) and (iii), respectively), was fractionated by Alexa-488-labeled Nef staining in (ii) and (iv). The counts within the M1 regions and the remaining parts of the total counts are defined as the fraction of Nef- positive (infected) and Nef-negative (target) cells, respectively.

### Rate of RNA degradation and loss of infectivity for SHIV-KS661 in the culture condition

The RNA degradation and thermal deactivation of SHIV-KS661 was measured by incubating 4 ml of stock virus, without cells, in a 35 mm Petri dish under the same conditions as the infection experiments (in RPMI-1640 medium supplemented with 10% fetal calf serum at 37°C and 5% $CO_2$ in humidified condition). Aliquots of the stock (500 μl) were sampled every day from day 0 to day 5 and stored at -80°C (see Figure 2). The RNA copy number and 50% tissue culture infectious dose of the samples were measured as described above.

### Mathematical model and fitting

We simultaneously fit Eqs.(5)-(8) to the concentration of Nef-negative and Nef-positive HSC-F cells and the infectious and total viral loads at four different MOIs (Figure 3) using nonlinear least-squares regression (FindMinimum package of *Mathematica7.0*) which minimizes the following objective function:

$$SSR = \sum_{j=1}^{4}\left[\sum_{i=1}^{9}\left\{\log x_j(t_i) - \log x_j^e(t_i)\right\}^2 + \sum_{i=1}^{9}\left\{\log y_j(t_i) - \log y_j^e(t_i)\right\}^2 + \sum_{i=1}^{9}\left\{\log v_{RNAj}(t_i) - \log v_{RNAj}^e(t_i)\right\}^2 + \sum_{i=1}^{9}\left\{\log v_{50j}(t_i) - \log v_{50j}^e(t_i)\right\}^2\right]$$

where $x_j(t_i)$, $y_j(t_i)$, $v_{RNAj}(t_i)$, and $v_{50j}(t_i)$ are the model-predicted values for Nef-negative cells, Nef-positive cells, total RNA viral load and infectious ($TCID_{50}$) viral load, given by the solution of Eqs.(5)-(8) at measurement time $t_i$ ($t_i$ = 0, 1, 2, ..., 8 d). Index $j$ is a label for the MOI of the four experiments (i.e., for MOI: $2.0 \times 10^{-3}$, $2.0 \times 10^{-4}$, $2.0 \times 10^{-5}$, and $2.0 \times 10^{-6}$). The variables with superscript "$e$" are the corresponding experimental measurements of those quantities. Note that the HSC-F cells were inoculated with SHIV-KS661 24 h before $t$ = 0. Experimental measurements below the detection limit (marked "d.l." in Table 1) were excluded when computing the *SSR*. Alternative fits with various weights on the infectious viral load to account for larger errors in the $TCID_{50}$ value [61], were also performed, but these did not significantly alter the extracted parameter values (Additional files 4, 5, 6, 7, 8, 9). To derive the 95% confidence interval for each parameter, we employed the

bootstrap method [62,63], estimating parameter values using 256 replicates of the four data sets and calculating the 2.5 and 97.5 percentiles.

## Additional material

**Additional file 1: Fit of a mathematical model which includes an eclipse phase of infection to experimental data of SHIV-KS661 *in vitro*.** Testing a variant of the model which incorporates an "eclipse" phase of infection to represent the cell's period of latency prior to virus production (see Additional file 2 for more detailed information).

**Additional file 2: Additional documentation for Additional files** 1. Detailed explanation of mathematical models used in Additional files 1.

**Additional file 3: Table for estimated parameters in Additional files** 1. Parameters values, initial values and derived quantities for the *in vitro* experiment with eclipse model.

**Additional file 4: Fit of the mathematical model with $SSR^W$ ($W$ = 0.0001) to experimental data of SHIV-KS661 *in vitro* (a).** Fitting with weight of $W = 0.0001$ on the infectious viral load to account for larger errors in the $TCID_{50}$ value (see Additional file 8 for more detailed information).

**Additional file 5: Fit of the mathematical model with $SSR^W$ ($W$ = 0.1) to experimental data of SHIV-KS661 *in vitro* (b).** Fitting with weight of $W = 0.1$ on the infectious viral load to account for larger errors in the $TCID_{50}$ value (see Additional file 8 for more detailed information).

**Additional file 6: Fit of the mathematical model with $SSR^W$ ($W$ = 10) to experimental data of SHIV-KS661 *in vitro* (c).** Fitting with weight of $W = 10$ on the infectious viral load to account for larger errors in the $TCID_{50}$ value (see Additional file 8 for more detailed information).

**Additional file 7: Fit of the mathematical model with $SSR^W$ ($W$ = 10000) to experimental data of SHIV-KS661 *in vitro* (d).** Fitting with weight of $W = 10000$ on the infectious viral load to account for larger errors in the $TCID_{50}$ value (see Additional file 8 for more detailed information).

**Additional file 8: Additional documentation for Additional files** 4, 5, 6, 7. Detailed explanation of mathematical models used in **Additional files** 4, 5, 6, 7.

**Additional file 9: Table for estimated parameters in Additional files** 4, 5, 6, 7. Parameters values and derived quantities for the *in vitro* experiment with various $SSR^W$s.

### List of abbreviations

SHIV: simian/human immunodeficiency virus; HIV-1: human immunodeficiency virus type-1; MDCK: Madin Darby canine kidney; HF: hollow-fiber; $IC_{50}$: 50% inhibitory concentration; HCV: hepatitis C virus; HA: hemagglutination assay; $TCID_{50}$: 50% tissue culture infection dose; PFU: plaque forming units; MOI: multiplicities of infection; PB: peripheral blood.

### Acknowledgements

This work was supported, in part, by JST PRESTO program (SI) and by the Natural Sciences and Engineering Research Council of Canada (CAAB) and by a grant-in-aid for scientific research from the Ministry of Education and Science, Japan, Research on Human Immunodeficiency Virus/AIDS in Health and Labor Sciences research grants from the Ministry of Health, Labor and Welfare, Japan, a research grant for health sciences focusing on drug innovation for AIDS from the Japan Health Sciences Foundation (TM).

### Author details

[1]Precursory Research for Embryonic Science and Technology (PRESTO), Japan Science and Technology Agency (JST), Kawaguchi, Saitama 332-0012, Japan. [2]Graduate School of Mathematical Sciences, The University of Tokyo, Meguro-ku, Tokyo 153-8914, Japan. [3]Institute for Virus Research, Kyoto University, Kyoto, Kyoto 606-8507, Japan. [4]Department of Physics, Ryerson University, ON, Toronto M5B 2K3, Canada. [5]Department of Systems Engineering, Shizuoka University, Hamamatsu, Shizuoka 432-8561, Japan. [6]Department of Biology, Faculty of Sciences, Kyushu University, 6-10-1 Hakozaki, Higashi-ku, Fukuoka, Fukuoka 812-8581, Japan.

### Authors' contributions

SI, KS, TI and TM designed the study.
SI, BPH and SM carried out data analysis.
TT and TM performed all experiments.
SI and CAAB developed mathematical model.
SI, BPH, CAAB and TM wrote the final manuscript.
All authors read and approved the final manuscript.

### Competing interests

The authors declare that they have no competing interests.

Received: 7 October 2011 Accepted: 25 February 2012
Published: 25 February 2012

### References

1. Harouse JM, Gettie A, Tan RC, Blanchard J, Cheng-Mayer C: **Distinct pathogenic sequela in rhesus macaques infected with CCR5 or CXCR4 utilizing SHIVs.** *Science* 1999, **284**:816-819.
2. Matsuda K, Inaba K, Fukazawa Y, Matsuyama M, Ibuki K, Horiike M, Saito N, Hayami M, Igarashi T, Miura T: ***In vivo* analysis of a new R5 tropic SHIV generated from the highly pathogenic SHIV-KS661, a derivative of SHIV-89.6.** *Virology* 2010, **399**:134-143.
3. Nishimura Y, Igarashi T, Donau OK, Buckler-White A, Buckler C, Lafont BA, Goeken RM, Goldstein S, Hirsch VM, Martin MA: **Highly pathogenic SHIVs and SIVs target different $CD4^+$ T cell subsets in rhesus monkeys explaining their divergent clinical courses.** *Proc Natl Acad Sci USA* 2004, **101**:12324-12329.
4. Reimann KA, Li JT, Veazey R, Halloran M, Park IW, Karlsson GB, Sodroski J, Letvin NL: **A chimeric simian/human immunodeficiency virus expressing a primary patient human immunodeficiency virus type 1 isolate env causes an AIDS-like disease after in vivo passage in rhesus monkeys.** *J Virol* 1996, **70**:6922-6928.
5. Shinohara K, Sakai K, Ando S, Ami Y, Yoshino N, Takahashi E, Someya K, Suzaki Y, Nakasone T, Sasaki Y, Kaizu M, Lu Y, Honda M: **A highly pathogenic simian/human immunodeficiency virus with genetic changes in cynomolgus monkey.** *J Gen Virol* 1999, **80**:1231-1240.
6. Kozyrev IL, Ibuki K, Shimada T, Kuwata T, Takemura T, Hayami M, Miura T: **Characterization of less pathogenic infectious molecular clones derived from acute-pathogenic SHIV-89.6p stock virus.** *Virology* 2001, **282**:6-13.
7. Miyake A, Ibuki K, Enose Y, Suzuki H, Horiuchi R, Motohara M, Saito N, Nakasone T, Honda M, Watanabe T, Miura T, Hayami M: **Rapid dissemination of a pathogenic simian/human immunodeficiency virus to systemic organs and active replication in lymphoid tissues following intrarectal infection.** *J Gen Virol* 2006, **13**:11-20.
8. Inaba K, Fukazawa Y, Matsuda K, Himeno A, Matsuyama M, Ibuki K, Miura Y, Koyanagi Y, Nakajima A, Blumberg RS, Takahashi H, Hayami M, Igarashi T, Miura T: **Small intestine $CD4^+$ cell reduction and enteropathy in simian/human immunodeficiency virus KS661-infected rhesus macaques in the presence of low viral load.** *J Gen Virol* 2010, **91**:773-781.
9. Dixit NM, Layden-Almer JE, Layden TJ, Perelson AS: **Modelling how ribavirin improves interferon response rates in hepatitis C virus infection.** *Nature* 2004, **432**:922-924.
10. Ho DD, Neumann AU, Perelson AS, Chen W, Leonard JM, Markowitz M: **Rapid turnover of plasma virions and CD4 lymphocytes in HIV-1 infection.** *Nature* 1995, **373**:123-126.
11. Little SJ, McLean AR, Spina CA, Richman DD, Havlir DV: **Viral dynamics of acute HIV-1 infection.** *J Exp Med* 1999, **190**:841-850.
12. Markowitz M, Louie M, Hurley A, Sun E, Di Mascio M, Perelson AS, Ho DD: **A novel antiviral intervention results in more accurate assessment of human immunodeficiency virus type 1 replication dynamics and T-cell decay in vivo.** *J Virol* 2003, **77**:5037-5038.
13. Neumann AU, Lam NP, Dahari H, Gretch DR, Wiley TE, Layden TJ, Perelson AS: **Hepatitis C viral dynamics in vivo and the antiviral efficacy of interferon-alpha therapy.** *Science* 1998, **282**:103-107.
14. Perelson AS, Essunger P, Cao Y, Vesanen M, Hurley A, Saksela K, Markowitz M, Ho DD: **Decay characteristics of HIV-1-infected compartments during combination therapy.** *Nature* 1997, **387**:188-191.

15. Perelson AS, Neumann AU, Markowitz M, Leonard JM, Ho DD: **HIV-1 dynamics in vivo: virion clearance rate, infected cell life-span, and viral generation time.** *Science* 1996, **271**:1582-1586.
16. Ribeiro RM, Qin L, Chavez LL, Li D, Self SG, Perelson AS: **Estimation of the initial viral growth rate and basic reproductive number during acute HIV-1 infection.** *J Virol* 2010, **84**:6096-6102.
17. Stafford MA, Corey L, Cao Y, Daar ES, Ho DD, Perelson AS: **Modeling plasma virus concentration during primary HIV infection.** *J Theor Biol* 2000, **203**:285-301.
18. Baccam P, Beauchemin C, Macken CA, Hayden FG, Perelson AS: **Kinetics of influenza A virus infection in humans.** *J Virol* 2006, **80**:7590-7599.
19. Beauchemin CA, McSharry JJ, Drusano GL, Nguyen JT, Went GT, Ribeiro RM, Perelson AS: **Modeling amantadine treatment of influenza A virus *in vitro*.** *J Theor Biol* 2008, **254**:439-451.
20. Chen HY, Di Mascio M, Perelson AS, Ho DD, Zhang L: **Determination of virus burst size in vivo using a single-cycle SIV in rhesus macaques.** *Proc Natl Acad Sci USA* 2007, **104**:19079-19084.
21. Dimitrov DS, Willey RL, Sato H, Chang LJ, Blumenthal R, Martin MA: **Quantitation of human immunodeficiency virus type 1 infection kinetics.** *J Virol* 1993, **67**:2182-2190.
22. Dinoso JB, Rabi SA, Blankson JN, Gama L, Mankowski JL, Siliciano RF, Zink MC, Clements JE: **A simian immunodeficiency virus-infected macaque model to study viral reservoirs that persist during highly active antiretroviral therapy.** *J Virol* 2009, **83**:9247-9257.
23. Igarashi T, Brown C, Azadegan A, Haigwood N, Dimitrov D, Martin MA, Shibata R: **Human immunodeficiency virus type 1 neutralizing antibodies accelerate clearance of cell-free virions from blood plasma.** *Nat Med* 1999, **5**:211-216.
24. Miao H, Hollenbaugh JA, Zand MS, Holden-Wiltse J, Mosmann TR, Perelson AS, Wu H, Topham DJ: **Quantifying the early immune response and adaptive immune response kinetics in mice infected with influenza A virus.** *J Virol* 2010, **84**:6687-6698.
25. Mitchell H, Levin D, Forrest S, Beauchemin CA, Tipper J, Knight J, Donart N, Layton RC, Pyles J, Gao P, Harrod KS, Perelson AS, Koster F: **Higher level of replication efficiency of 2009 (H1N1) pandemic influenza virus than those of seasonal and avian strains: kinetics from epithelial cell culture and computational modeling.** *J Virol* 2011, **85**:1125-1135.
26. Mohler L, Flockerzi D, Sann H, Reichl U: **Mathematical model of influenza A virus production in large-scale microcarrier culture.** *Biotechnol Bioeng* 2005, **90**:46-58.
27. Nowak MA, Lloyd AL, Vasquez GM, Wiltrout TA, Wahl LM, Bischofberger N, Williams J, Kinter A, Fauci AS, Hirsch VM, Lifson JD: **Viral dynamics of primary viremia and antiretroviral therapy in simian immunodeficiency virus infection.** *J Virol* 1997, **71**:7518-7525.
28. Regoes RR, Barber DL, Ahmed R, Antia R: **Estimation of the rate of killing by cytotoxic T lymphocytes in vivo.** *Proc Natl Acad Sci USA* 2007, **104**:1599-1603.
29. Schulze-Horsel J, Schulze M, Agalaridis G, Genzel Y, Reichl U: **Infection dynamics and virus-induced apoptosis in cell culture-based influenza vaccine production - Flow cytometry and mathematical modeling.** *Vaccine* 2009, **27**:2712-2722.
30. Funk GA, Fischer M, Joos B, Opravil M, Gunthard H, Huldrych F, Ledergerber B, Bonhoeffer S: **Quantification of In Vivo Replicative Capacity of HIV-1 in Different Compartments of Infected Cells.** *JAIDS* 2001, **26**:397-404.
31. Hlavacek WS, Stilianakis NI, Notermans DW, Danner SA, Perelson AS: **Influence of follicular dendritic cells on decay of HIV during antiretroviral therapy.** *Proc Natl Acad Sci USA* 2000, **97**:10966-10971.
32. Kepler GM, Nguyen HK, Webster-Cyriaque J, Banks HT: **A dynamic model for induced reactivation of latent virus.** *J Theor Biol* 2007, **244**:451-462.
33. Murray JM, Purcell RH, Wieland SF: **The half-life of hepatitis B virions.** *Hepatology* 2006, **44**:1117-1121.
34. Regoes RR, Antia R, Garber DA, Silvestri G, Feinberg MB, Staprans SI: **Roles of target cells and virus-specific cellular immunity in primary simian immunodeficiency virus infection.** *J Virol* 2004, **78**:4866-4875.
35. Speirs C, van Nimwegen E, Bolton D, Zavolan M, Duvall M, Angleman S, Siegel R, Perelson AS, Lenardo MJ: **Analysis of human immunodeficiency virus cytopathicity by using a new method for quantitating viral dynamics in cell culture.** *J Virol* 2005, **79**:4025-4032.
36. Stilianakis NI, Boucher CAB, deJong MD, van Leeuwen R, Schuurman R, de Boer RJ: **Clinical data sets of HIV1 Reverse transcriptase-resistant mutants explained by a mathematical model.** *J Virol* 1997, **71**:161-168.
37. Verotta D, Schaedeli F: **Non-linear dynamics modes characterizing long-term virological data from AIDS clinical trials.** *Math Biosci* 2002, **176**:163-183.
38. Nowak MA, May RM: **Virus dynamics.** Oxford University Press; 2000.
39. Perelson AS: **Modeling viral and immune system dynamics.** *Nat Rev Immunol* 2001, **2**:28-36.
40. Bangham CRM, Kirkwood TBL: **Defective interfering particles: Effects in modulating virus growth and persistence.** *Virology* 1990, **179**:821-826.
41. Ma ZM, Stone M, Piatak M, Schweighardt B, Haigwood NL, Montefiori D, Lifson JD, Busch MP, Miller CJ: **High specific infectivity of plasma virus from the pre-ramp-up and ramp-up stages of acute Simian Immunodeficiency Virus infection.** *J Virol* 2009, **83**:3288-3297.
42. Vaidya NK, Ribeiro RM, Miller CJ, Perelson AS: **Viral dynamics during primary Simian Immunodeficiency Virus Infection: Effect of Time-dependent Virus Infectivity.** *J Virol* 2010, **84**:4302-4310.
43. Anderson RM: **The Kermack-McKendrick Epidemic Threshold Theorem.** *Bull Math Biol* 1991, **53**:3-32.
44. Brandin E, Thorstensson R, Bonhoeffer S, Albert J: **Rapid viral decay in simian immunodeficiency virus-infected macaques receiving quadruple antiretroviral therapy.** *J Virol* 2006, **80**:9861-9864.
45. Eckstein DA, Penn ML, Korin YD, Scripture-Adams DD, Zack JA, Kreisberg JF, Roederer M, Sherman MP, Chin PS, Goldsmith MA: **HIV-1 actively replicates in naive CD4(+) T cells residing within human lymphoid tissues.** *Immunity* 2001, **15**:671-682.
46. Tsai WP, Conley SR, Kung HF, Garrity RR, Nara PL: **Preliminary in vitro growth cycle and transmission studies of HIV-1 in an autologous primary cell assay of blood-derived macrophages and peripheral blood mononuclear cells.** *Virology* 1996, **226**:205-216.
47. Huang AS, Baltimore D: **Defective viral particles and viral disease processes.** *Nature* 1970, **226**:325-327.
48. Kwon YJ, Hung G, Anderson WF, Peng CA, Yu H: **Determination of infectious retrovirus concentration from colony-forming assay with quantitative analysis.** *J Virol* 2003, **77**:5712-5720.
49. Rusert P, Fischer M, Joos B, Leemann C, Kuster H, Flepp M, Bonhoeffer S, Gunthard HF, Trkola A: **Quantification of infectious HIV-1 plasma viral load using a boosted in vitro infection protocol.** *Virology* 2004, **326**:113-129.
50. Platt EJ, Kozak SL, Durnin JP, Hope TJ, Kabat D: **Rapid dissociation of HIV-1 from cultured cells severely limits infectivity assays, causes the inactivation ascribed to entry inhibitors, and masks the inherently high level of infectivity of virions.** *J Virol* 2010, **84**:3106-3110.
51. Thomas JA, Ott DE, Gorelick RJ: **Efficiency of Human Immunodeficiency Virus Type 1 Postentry Infection Processes: Evidence against Disproportionate Numbers of Defective Virions.** *J Virol* 2007, **81**:4367-4370.
52. Marcus PI, Ngunjiri JM, Sekellick MJ: **Dynamics of biologically active subpopulations of influenza virus: Plaque-forming, noninfectious cell-killing, and defective interfering particles.** *J Virol* 2009, **83**:8122-8130.
53. Izumi T, Io K, Matsui M, Shirakawa K, Shinohara M, Nagai Y, Kawahara M, Kobayashi M, Kondoh H, Misawa N, Koyanagi Y, Uchiyama T, Takaori-Kondo A: **HIV-1 viral infectivity factor interacts with TP53 to induce G2 cell cycle arrest and positively regulate viral replication.** *Proc Natl Acad Sci USA* 2010, **107**:20798-20803.
54. Sato K, Izumi T, Misawa N, Kobayashi T, Yamashita Y, Ohmichi M, Ito M, Takaori-Kondo A, Koyanagi Y: **Remarkable lethal G-to-A mutations in vif-proficient HIV-1 provirus by individual APOBEC3 proteins in humanized mice.** *J Virol* 2010, **84**:9546-9556.
55. De Jong MD, Simmons CP, Thanh TT, Hien VM, Smith GJD, Chau TNB, Hoang DM, Chau NVV, Khanh TH, Dong VC, Qui PT, Cam BV, Ha DQ, Guan Y, Peiris JSM, Chinh NT, Hien TT, Farrar J: **Fatal outcome of human influenza A (H5N1) is associated with high viral load and hypercytokinemia.** *Nat Med* 2006, **12**:1203-1207.
56. Wakita T, Pietschmann T, Kato T, Date T, Miyamoto M, Zhao Z, Murthy K, Habermann A, Kräusslich HG, Mizokami M, Bartenschlager R, Liang TJ: **Production of infectious hepatitis C virus in tissue culture from a cloned viral genome.** *Nat Med* 2005, **11**:791-796.
57. Watashi K, Ishii N, Hijikata M, Inoue D, Murata T, Miyanari Y, Shimotohno K: **Cyclophilin B is a functional regulator of hepatitis C virus RNA polymerase.** *Mol Cell* 2005, **19**:111-122.

58. Clapham PR, Weiss RA, Dalgleish AG, Exley M, Whitby D, Hogg N: **Human immunodeficiency virus infection of monocytic and T-lymphocytic cells: receptor modulation and differentiation induced by phorbol ester.** *Virology* 1987, **158**:44-51.
59. Akari H, Mori K, Terao K, Otani I, Fukasawa M, Mukai R, Yoshikawa Y: ***In vitro* immortalization of Old World monkey T lymphocytes with Herpesvirus saimiri: its susceptibility to infection with simian immunodeficiency viruses.** *Virology* 1996, **218**:382-388.
60. Reed LJ, Muench H: **A simple method of estimating fifty per cent endpoints.** *Am J Hyg* 1938, **27**:493-497.
61. Macken C: **Design and analysis of serial limiting dilution assays with small sample sizes.** *J Immunol Methods* 1999, **222**:13-29.
62. Efron B: **Bootstrap Method: Another Look at the Jackknife.** *Annals of Statistic* 1979, **7**:1-26.
63. Efron B, Tibshirani R: **Bootstrap methods for standard errors, confidence intervals, and other measures of statistical accuracy.** *Stat Sci* 1986, 1:54-75.

doi:10.1186/PREACCEPT-8502330256154242
**Cite this article as:** Iwami *et al.*: Quantification system for the viral dynamics of a highly pathogenic simian/human immunodeficiency virus based on an *in vitro* experiment and a mathematical model. *Retrovirology* 2012 **9**:18.

JVI
Journals.ASM.org

# Molecular Requirements for T Cell Recognition of N-Myristoylated Peptides Derived from the Simian Immunodeficiency Virus Nef Protein

**Daisuke Morita,[a,b] Yukie Yamamoto,[a] Juri Suzuki,[c] Naoki Mori,[d] Tatsuhiko Igarashi,[b] Masahiko Sugita[a]**

Laboratory of Cell Regulation[a] and Laboratory of Primate Model,[b] Institute for Virus Research, Kyoto University, Kyoto, Japan; Center for Human Evolution Modeling Research, Primate Research Institute, Kyoto University, Aichi, Japan[c]; Division of Applied Life Sciences, Graduate School of Agriculture, Kyoto University, Kyoto, Japan[d]

**We have recently isolated a rhesus macaque cytotoxic T cell line, 2N5.1, that specifically recognizes an N-myristoylated 5-mer peptide ($C_{14}$-Gly-Gly-Ala-Ile-Ser [C14nef5]) derived from the simian immunodeficiency virus (SIV) Nef protein. Such C14nef5-specific T cells expand in the circulation of SIV-infected monkeys, underscoring the capacity of T cells to recognize viral lipopeptides; however, the molecular basis for the lipopeptide antigen presentation remains to be elucidated. Here, functional studies indicated that the putative antigen-presenting molecule for 2N5.1 was likely to have two separate antigen-binding sites, one for interaction with a $C_{14}$-saturated acyl chain and the other for anchorage of the C-terminal serine residue. Mutants with alanine substitutions for the second glycine residue and the fourth isoleucine residue were not recognized by 2N5.1 but interfered with the presentation of C14nef5 to 2N5.1, indicating that these structural analogues retained the ability to interact with the antigen-presenting molecules. In contrast to the highly specific recognition of C14nef5 by 2N5.1, an additional cytotoxic T cell line, SN45, established independently from a C14nef5-stimulated T cell culture, showed superb reactivity to both C14nef5 and an N-myristoylated Nef 4-mer peptide, and therefore, the C-terminal serine residue was dispensable for the recognition of lipopeptides by the SN45 T cells. Furthermore, the mutants with alanine substitutions were indeed recognized by the SN45 T cells. Given that N-myristoylation of the Nef protein occurs in the conserved motifs and is critical for viral pathogenesis, these observations predict that the lipopeptide-specific T cell response is difficult for viruses to avoid by simply introducing amino acid mutations.**

Modern immunology has established a central paradigm for antigen (Ag) presentation that major histocompatibility complex (MHC) class I and class II molecules bind peptide Ags and present them to $CD8^+$ and $CD4^+$ T cells, respectively (1). The important role of MHC-restricted T cells in various aspects of acquired immunity has been noted, and effective protein vaccines have been developed to control many infectious diseases. Subsequently, the repertoire of Ags recognized by T cells has been expanded to include not only proteins, but also lipidic molecules. Human group 1 CD1 molecules (CD1a, -b, and -c) are capable of binding glycolipids and presenting them to T cells. Such glycolipid-specific group 1 CD1-restricted T cells have been shown to expand significantly in response to mycobacterial infections, and a role for them in controlling intracellular microbes has been suggested (2–5).

Unlike bacteria, viruses do not possess their own lipids, and thus, lipid-specific adaptive immunity may not function efficiently against viral infections. However, viruses can indeed biosynthesize their own lipopeptides by utilizing the host cellular machinery. Human (HIV) and simian (SIV) immunodeficiency viruses borrow the host-derived *N*-myristoyl-transferase and its substrate, myristoyl-coenzyme A (CoA), for coupling a saturated $C_{14}$ fatty acid (myristic acid) to the N-terminal glycine residue of the Nef protein (6). This lipidation reaction, referred to as N-myristoylation, is a key modification for anchoring the Nef protein to the plasma membrane, thereby assisting its immunosuppressive activity (7). Interestingly, our previous study indicated that the host-acquired immunity was equipped with cytotoxic T cells capable of monitoring the N-myristoylation of the Nef protein (8). A rhesus macaque $CD8^+$ T cell line, 2N5.1, specifically recognized an N-myristoylated, but not unmodified, 5-mer peptide of the SIV Nef protein. Furthermore, the number of N-myristoylated Nef peptide-specific T cells was increased significantly in the circulation of SIV-infected monkeys, and the plasma viral load in infected monkeys was found to correlate reciprocally with the number of lipopeptide-specific T cells (8). Taken together, these results point to an intriguing possibility that, in addition to peptides and lipids, viral lipopeptides may comprise a new repertoire of Ags recognized by host T cells.

To gain insight into the molecular basis for lipopeptide Ag presentation, we established an additional $CD8^+$ T cell line, SN45, independent of 2N5.1, that recognized the same N-myristoylated 5-mer peptide. A comparative study of the two T cell lines detected different molecular patterns for the recognition of lipopeptide Ags. Strikingly, the mutant with a C-terminal serine deletion and the mutants with alanine substitutions of the N-myristoylated 5-mer peptide were recognized by the SN45 T cells, suggesting that pathogenic viruses may find difficulties in escaping from the lipopeptide-specific T cell responses by simply introducing amino acid mutations.

Received 13 August 2012 Accepted 15 October 2012
Published ahead of print 24 October 2012
Address correspondence to Masahiko Sugita, msugita@virus.kyoto-u.ac.jp, or Tatsuhiko Igarashi, tigarash@virus.kyoto-u.ac.jp.

doi:10.1128/JVI.02142-12

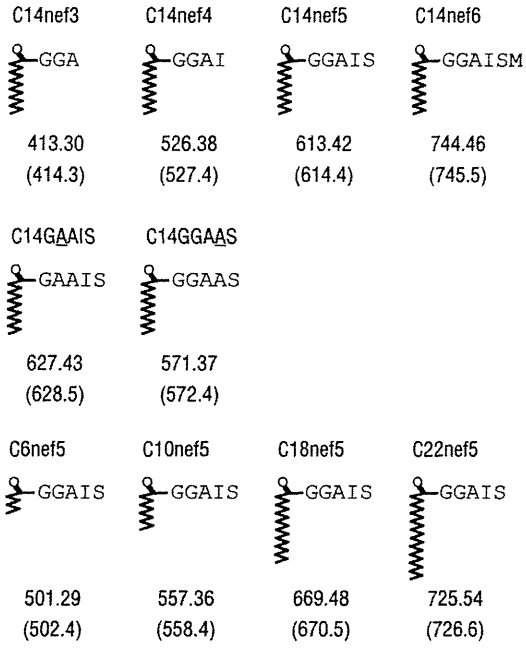


FIG 1 Synthetic lipopeptides used in this study. The names and the chemical structures are shown. The monoisotopic mass of each compound, as well as the observed *m/z* of the $[M + H]^+$ (in parentheses), are also shown.

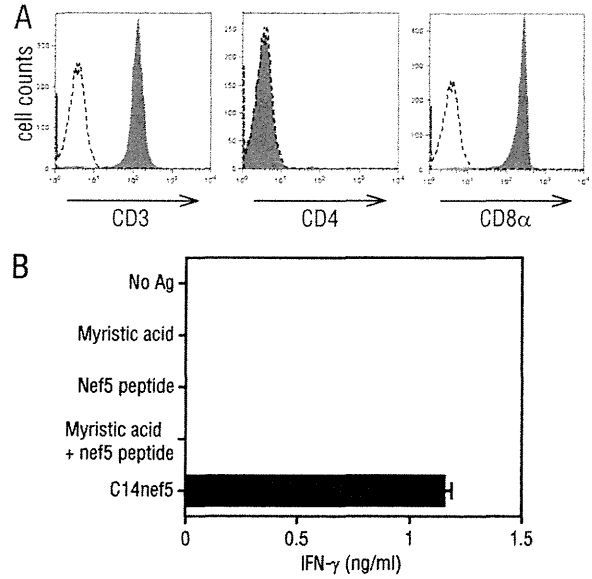


FIG 2 Specific recognition of C14nef5 by SN45. (A) The surface expression of T cell markers was analyzed for SN45 by flow cytometry (filled histograms). A dashed line in each panel indicates a negative-control histogram. (B) SN45 T cells ($5 \times 10^4$/well) were stimulated with the indicated Ags (5 μg/ml) in the presence of irradiated autologous PBMCs ($3 \times 10^5$/well), and the amount of IFN-γ released into the culture medium was measured. Assays were performed in triplicate, and mean values and standard deviations (SD) are shown.

## MATERIALS AND METHODS

**Synthesis of lipopeptide Ags.** Chemical reagents were purchased from Nacalai Tesque (Kyoto, Japan) unless otherwise indicated. The lipopeptide Ags listed in Fig. 1 were synthesized as described previously (8). Briefly, peptides were synthesized by a manual 9-fluorenylmethoxy carbonyl (Fmoc) solid-phase peptide synthesis technique using Wang resin precoupled with a relevant C-terminal amino acid (EMD Chemicals, Gibbstown, NJ). Acylation was carried out by reacting the N-terminal amino acid group with acid anhydrides prepared with *N,N'*-diisopropylcarbodiimide, followed by the release of the acylated peptides in 95% trifluoroacetic acid. Purification of the crude samples was performed by high-performance liquid chromatography (HPLC) with a gradient elution based on water and methanol with 0.1% trifluoroacetic acid. After freeze-drying, the purified samples were subjected to liquid chromatography (LC)-mass spectrometry, using a $C_{18}$ column (GL Sciences, Torrance, CA) with a solvent system of water and methanol with 0.1% formic acid. The observed *m/z* of the $[M + H]^+$ for each purified sample was consistent with the monoisotopic mass (Fig. 1), thus confirming the identity of the synthesized lipopeptides.

**Establishment of lipopeptide-specific rhesus macaque T cell lines and flow cytometric analysis.** The $C_{14}$-Gly-Gly-Ala-Ile-Ser (C14nef5)-specific T cell line 2N5.1 was described previously (8). Another C14nef5-specific T cell line, SN45, was obtained independently from a SIV-infected monkey (MM521). Peripheral blood mononuclear cells (PBMCs) ($1.2 \times 10^7$/well) were cultured with C14nef5 at a concentration of 5 μg/ml, and antigenic stimulation was repeated every 2 weeks in the presence of irradiated autologous PBMCs. Interleukin 2 (IL-2) was added at 0.3 nM after the second stimulation, and the concentration was gradually increased to 3 nM by the fourth stimulation. RPMI 1640 medium (Invitrogen, Carlsbad, CA) supplemented with 10% heat-inactivated fetal calf serum (FCS) (HyClone, Logan, UT), 2-mercaptoethanol (Invitrogen), penicillin, and streptomycin was used for T cell culture. The expression of T cell markers on the T cell line was analyzed by flow cytometry, as described previously (8).

**T cell assays.** T cells ($5 \times 10^4$/well) were incubated with each synthetic lipopeptide (5 μg/ml) in the presence of irradiated autologous or allogeneic PBMCs ($3 \times 10^5$/well), using 96-well flat-bottom microtiter plates. In some experiments, irradiated allogeneic PBMCs ($2 \times 10^5$/well) were preincubated for 30 min with test competitors (0.5 μg/ml or 5 μg/ml), and then, responder T cells ($5 \times 10^4$/well) and C14nef5 (50 ng/ml) were added. After 24 h, aliquots of the culture supernatants were collected, and the amount of either gamma interferon (IFN-γ) or granulocyte-macrophage colony-stimulating factor (GM-CSF) released into the medium was measured using Mabtech ELISA kits (Nacka Strand, Sweden). To examine if the T cell response might be mediated by MHC or CD1 molecules, PBMCs ($3 \times 10^5$/well) were incubated with saturating amounts (5 μg/ml) of monoclonal antibodies (Abs) to CD1a (10H3), CD1b (b3.1), CD1c (M241), MHC class I (W6/32), and MHC class II (L243) or negative-control Ab (P3) for 20 min before the addition of responder T cells ($5 \times 10^4$/well) and the C14nef5 Ag (5 μg/ml). Alternatively, the LLC-MK2 rhesus macaque kidney epithelial cell line was transiently transfected with rhesus macaque group 1 CD1 genes (*CD1A*, *CD1B*, and *CD1C*) (9) or MM521-derived MHC class I genes (*Mamu-A1*02*, *Mamu-A1*110*, and *Mamu-B*56*) and used as Ag-presenting cells ($2.5 \times 10^4$/well) in the T cell assays described above.

**TCR cloning.** T-cell receptor (TCR) cloning was performed by the inverse-PCR method (10, 11). Briefly, total RNA was extracted from $1 \times 10^6$ T cells, and oligo(dT)-primed double-stranded cDNA was synthesized from 0.25 μg of the total RNA using PrimeScript reverse transcriptase (TaKaRa Bio, Inc., Otsu, Japan), RNase H (New England BioLabs, Inc., Ipswich, MA), *Escherichia coli* DNA polymerase I (New England BioLabs, Inc.), and *E. coli* DNA ligase (New England BioLabs, Inc.), followed by treatment with T4 DNA polymerase (New England BioLabs, Inc.) for blunt-end formation. The blunt-ended DNA was then circularized with T4 DNA ligase (New England BioLabs, Inc.) and used as a template for inverse PCR with a pair of Cα- or Cβ-specific primers oriented in opposite directions. The primers used were as follows: TCRα forward, 5′-GGG TCG ACG ACC TCA TGT CTA GCA CAG T-3′; TCRα reverse, 5′-GCA TGC GGC CGC CCT GCT ATG CTG TGT ATC-3′; TCRβ forward, 5′-GGG TCG ACA CAG CGA CCT TGG GTG GG-3′; TCRβ reverse, 5′-GCA TGC GGC CGC GGT CAA GAG AAA GGA TTC-3′. The

TABLE 1 TCR usage of 2N5.1 and SN45

| T cell line | Genes | Sequence[a] Vα | Vβ | Junction | Jα | Jβ |
|---|---|---|---|---|---|---|
| TCRα | | | | | | |
| 2N5.1 | TRAV35–TRAJ54 | GTYFCAG | | QNW | GAQKLVFG | |
| SN45 | TRAV4–TRAJ6 | VYYCLVG | | | GGGYVLTFG | |
| TCRβ | | | | | | |
| 2N5.1 | TRBV27–TRBJ27 | | YLCASSY | SGQA | | YEQYFGP |
| SN45 | TRBV3–TRBJ27 | | YFCASSQ | DLGAGEV | | YEQYFGP |

[a] The TCR usage of the two T cell lines was determined by inverse PCR, and the deduced amino acid sequences of the junctional regions are shown.

amplified TCR genes were cloned into pBlueScript II (Stratagene, La Jolla, CA). More than 10 clones were sequenced, using the BigDye Terminator v3.1 Cycle Sequencing Kit (Applied Biosystems, Carlsbad, CA).

**Animals.** The rhesus macaques (*Macaca mulatta*) used in this study were treated humanely in accordance with institutional regulations, and the experimental protocols were approved by the Committee for Experimental Use of Non-Human Primates at the Institute for Virus Research, Kyoto University. For infection, SIVmac239 (12) was inoculated intravenously at a dose of 2,000 50% tissue culture-infective doses ($TCID_{50}$).

**Nucleotide sequence accession numbers.** Sequences were deposited in the DDBJ/GenBank/EMBL databases under the following accession numbers: AB701289 (2N5.1 α chain), AB701290 (2N5.1 β chain), AB701291 (SN45 α chain), and AB701292 (SN45 β chain).

## RESULTS

**Establishment of an additional C14nef-specific T cell line, SN45.** We had previously isolated a rhesus monkey T cell line, 2N5.1, that specifically recognized the N-myristoylated 5-mer lipopeptide (C14nef5) derived from the SIV Nef protein (8). Another C14nef5-specific T cell line, termed SN45, was obtained independently by repeated stimulation of rhesus macaque PBMCs with C14nef5. As for 2N5.1 (8), the SN45 T cells were $CD4^-$ and $CD8\alpha^+$ (Fig. 2A), and produced IFN-γ in response to C14nef5, but no response was observed when myristic acid and the 5-mer peptide were added as a free form (Fig. 2B). Therefore, the SN45 T cells specifically recognized the 5-mer peptide that was conjugated covalently with myristic acid.

The TCR usage of 2N5.1 and SN45 was determined by inverse PCR, in which the TCR genes were randomly cloned and sequenced. For both T cell lines, a single pair of TCR α and β chains was detected, suggesting that the cell lines were clonal. Both T cell lines expressed distinct Vα and Vβ families and exhibited clono-

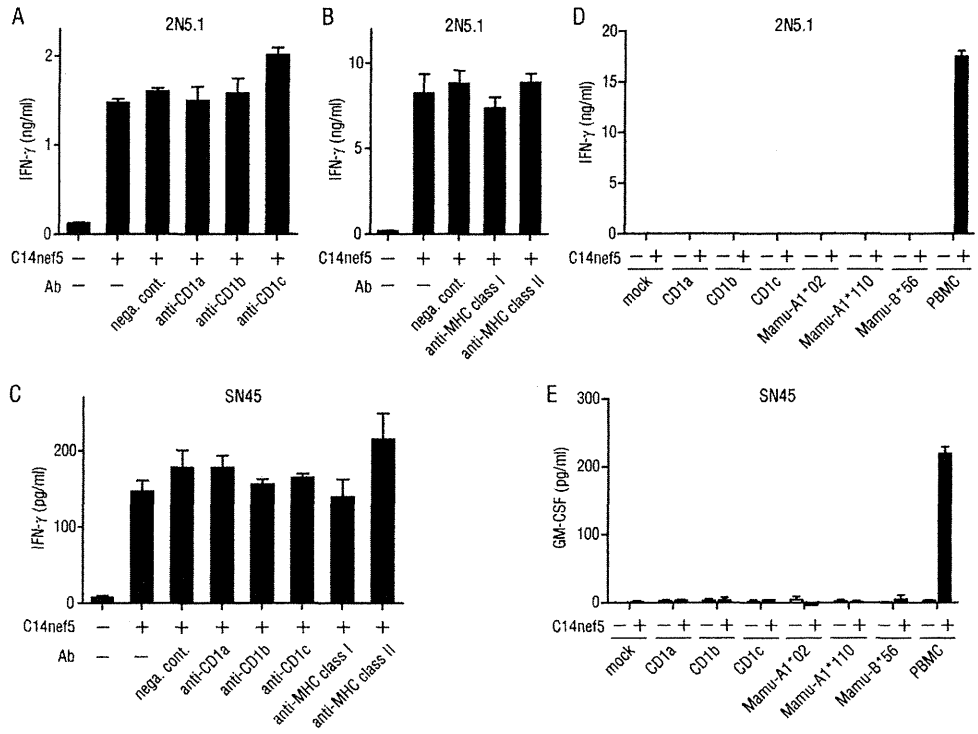


FIG 3 Involvement of MHC and CD1 molecules in the recognition of C14nef5 by 2N5.1 and SN45. Autologous PBMCs ($3 \times 10^5$/well) were preincubated with a saturating amount (5 μg/ml) of the indicated Abs and cultured with 2N5.1 (A and B) and SN45 (C) T cells ($5 \times 10^4$/well) in the presence (+) or absence (−) of C14nef5 (5 μg/ml). Note that these Abs were used to block relevant human T cell responses specifically and are known to recognize the corresponding monkey molecules efficiently (9, 23–26). nega. cont., negative control. (D and E) The LLC-MK2 rhesus macaque cell line was transiently transfected by lipofection with rhesus macaque CD1 genes or MM521-derived MHC class I genes (*Mamu-A1*02*, *Mamu-A1*110*, and *Mamu-B*56*) and tested for the ability to present C14nef5 to 2N5.1 (D) and SN45 (E). The transfection efficiency was approximately 50%, as determined by flow cytometric analysis of CD1-transfected cells labeled with relevant anti-CD1 Abs. The error bars indicate standard deviation (SD).

typic variations in the junctional region, except for the SN45 TCRα chain, which was germ line encoded without N additions (Table 1). Therefore, the recognition of the C14nef5 lipopeptide by 2N5.1 is unlikely to be mediated by invariant-type TCRs. It remains to be addressed whether SN45 may represent a new subset of semi-invariant TCR-expressing cells, but obviously, the cells are distinct from the CD1d-restricted, $V\alpha24^+$ natural killer (NK) T cells (13). Ab-blocking experiments suggested that none of the classical MHC molecules and group 1 CD1 molecules could mediate the lipopeptide Ag presentation to 2N5.1 (Fig. 3A and B) and SN45 (Fig. 3C). Furthermore, rhesus macaque cell transfectants expressing rhesus macaque group 1 CD1 molecules (CD1a, CD1b, and CD1c) and those expressing MM521-derived MHC class I molecules (Mamu-A1*02, Mamu-A1*110, and Mamu-B*56) failed to present C14nef5 to the T cell lines (Fig. 3D and E). Therefore, the molecular identity of the Ag-presenting molecules for the C14nef5 lipopeptide has not yet been determined, but as shown below, functional studies predicted that two discernible molecules exist in rhesus macaques that are capable of presenting N-myristoylated peptides to T cells.

**2N5.1, but not SN45, was stimulated by all the donors tested.** While the presentation of peptide Ags to T cells is mediated by highly polymorphic MHC molecules, the activation of glycolipid-specific T cells depends on non-MHC-encoded molecules of the CD1 family that are virtually monomorphic. To gain insight into the yet unidentified Ag-presenting molecules for the C14nef5 lipopeptide, we wished to determine if the restriction elements for the two lipopeptide-specific T cell lines might be shared functionally among individuals. Allogeneic PBMCs derived from all 9 donor rhesus macaques tested could present the C14nef5 lipopeptide Ag to 2N5.1 (Fig. 4A). In sharp contrast, only a single donor (MM460), and not the other 2 donors (MM450 and MM499), was capable of presenting C14nef5 to SN45 (Fig. 4B). The superb capacity of MM450- and MM499-derived PBMCs to present Ag to T cells was confirmed by demonstrating that the two donors were able to present C14nef5 to 2N5.1 (Fig. 4A). Studies of 8 additional monkeys revealed that two donors (MM1774 and MM1795), but not the other 6, could present the Ag to SN45 (Fig. 4C), indicating that the capacity to activate SN45 was not shared broadly among the subjects. Thus, these results suggested that the Ag-presenting molecules for 2N5.1 and SN45 were different.

**Distinct patterns of Ag recognition by 2N5.1 and SN45.** We then compared the two C14nef5-specific T cell lines in terms of their abilities to recognize an array of related compounds. We first examined whether the T cell lines might differentially recognize Ags with altered peptide lengths and amino acid compositions. Both cell lines were obtained by repeated stimulation with C14nef5 in an *in vitro* culture, and the 2N5.1 T cells faithfully recognized C14nef5, but not N-myristoylated 3-mer (C14nef3; $C_{14}$-GGA), 4-mer (C14nef4; $C_{14}$-GGAI), and 6-mer (C14nef6; $C_{14}$-GGAISM) peptides of the Nef protein (Fig. 5A, left) (8). Furthermore, an alanine substitution (underlined) for either the second glycine residue ($C_{14}$-G<u>A</u>AIS) or the isoleucine residue ($C_{14}$-GGA<u>A</u>S) of C14nef5 resulted in total abrogation of the antigenic activity (Fig. 5B, left) (8). In sharp contrast, the SN45 T cells recognized C14nef4, as well as C14nef5 (Fig. 5A, right), and were capable of reacting to the mutated Ags, albeit less efficiently to $C_{14}$-GGA<u>A</u>S (Fig. 5B, right).

We next addressed whether the length of the acyl chain impacts the efficiency of T cell activation. Pentamer Nef peptides conjugated with either shorter saturated fatty acids (C6nef5 and C10nef5) or longer saturated fatty acids (C18nef5 and C22nef5) were synthesized and tested for the ability to stimulate the T cell lines. As shown in Fig. 5C, both 2N5.1 (top) and SN45 (bottom) exhibited the highest reactivity to the authentic Ag with a saturated $C_{14}$ fatty acid. It was also noted that, whereas SN45 failed to respond to any of the altered Ags tested (Fig. 5C, bottom), 2N5.1 showed moderate reactivity to C10nef5 (Fig. 5C, top).

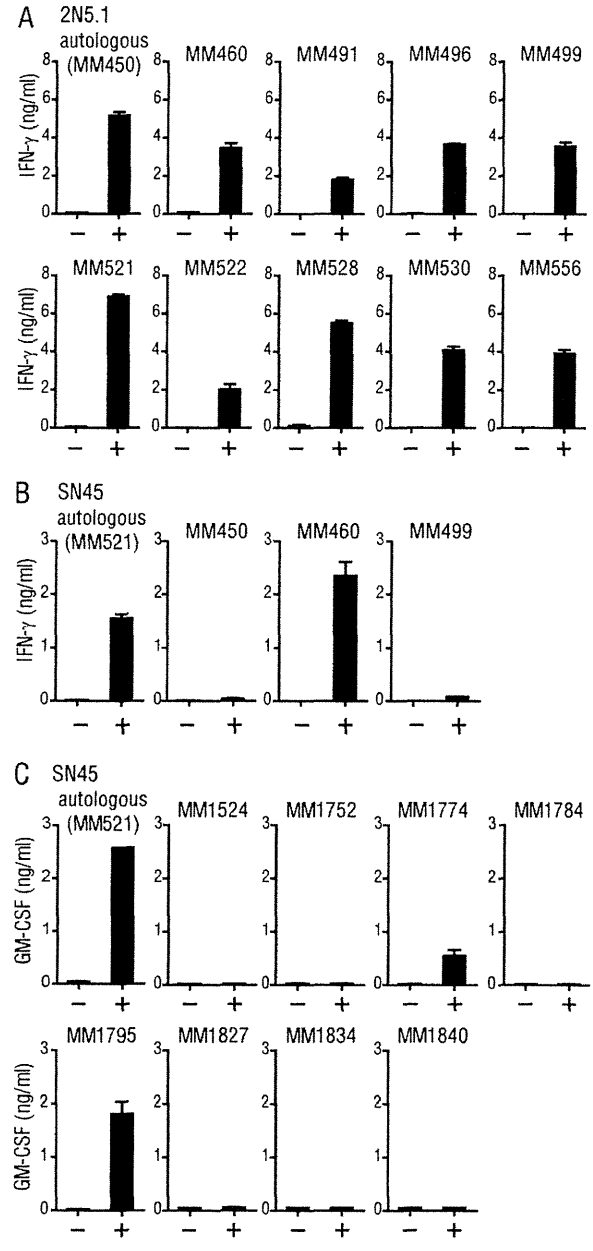


FIG 4 Responses of 2N5.1 and SN45 to C14nef5 in the presence of either autologous or allogeneic PBMCs. MM450-derived 2N5.1 T cells (A) and MM521-derived SN45 T cells (B) were stimulated with C14nef5 (+) or unstimulated (−) in the presence of irradiated autologous or allogeneic PBMCs. The amount of IFN-γ released into the medium was measured as for Fig. 2B. (C) For SN45, additional studies were performed with 8 allogeneic donors, and the amount of GM-CSF released into the medium was measured. The error bars indicate SD.

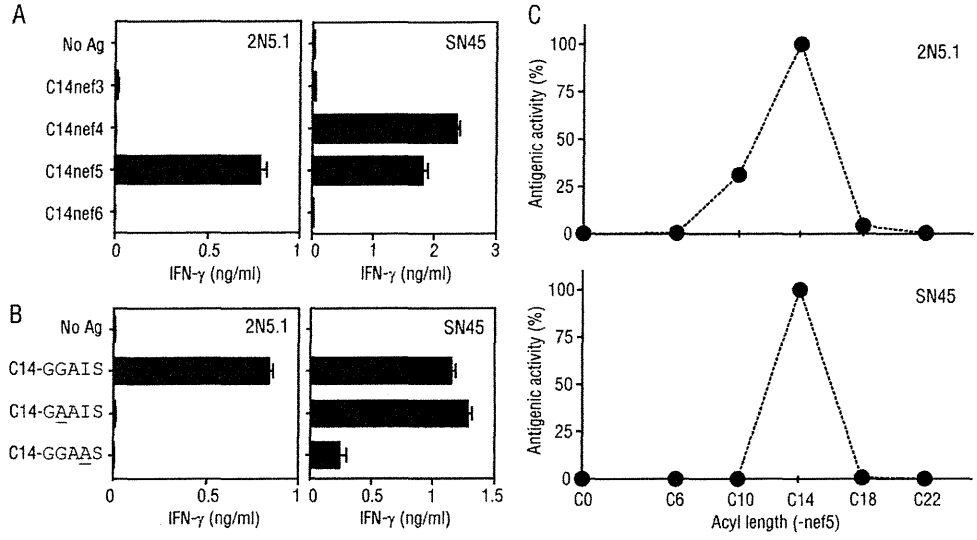


FIG 5 Responses of 2N5.1 and SN45 to an array of synthetic lipopeptides. (A) 2N5.1 (left) and SN45 (right) T cells were stimulated with either the N-myristoylated Nef 3-mer (C14nef3), 4-mer (C14nef4), 5-mer (C14nef5), or 6-mer (C14nef6) peptide, and the IFN-γ response of the T cells was measured. (B) T cells were stimulated with C14nef5 ($C_{14}$-GGAIS) or each of the mutants with alanine substitutions ($C_{14}$-GAAIS and $C_{14}$-GGAAS), and the IFN-γ response of the T cells was measured. The error bars indicate SD. (C) 2N5.1 (top) and SN45 (bottom) T cells were stimulated with a Nef 5-mer peptide that was either unconjugated ($C_0$) or conjugated with a saturated $C_6$, $C_{10}$, $C_{14}$, $C_{18}$, or $C_{22}$ fatty acid, and the IFN-γ response of the T cells was assessed. The ratio of each response to the response to C14nef5 is shown as the antigenic activity.

**A role for the C14nef5 serine residue in lipopeptide Ag presentation.** SN45 recognized both C14nef4 and C14nef5 (Fig. 5A), suggesting that the C-terminal serine residue of C14nef5 was dispensable for the activation of the T cells. On the other hand, 2N5.1 recognized C14nef5, but not C14nef4 (Fig. 5A), which pointed to a critical role for the serine residue either as an anchoring residue, as part of the T cell epitope, or both. We favored the hypothesis that the serine residue of C14nef5 functions as an anchoring residue because it was shared among many N-myristoylated proteins. We reasoned that if this was the case, even an excess amount of C14nef4 could not replace C14nef5 at the Ag-binding site. To address this directly, Ag-presenting cells were preincubated with excess amounts of C14nef4, and then the 2N5.1 T cells and the authentic C14nef5 Ag were added to the culture. As predicted, C14nef4 ($C_{14}$-GGAI) failed to interfere with the 2N5.1 T cell response to C14nef5 (Fig. 6A). In sharp contrast, preincubation with excess amounts of the mutants with alanine substitutions (underlined) ($C_{14}$-GAAIS and $C_{14}$-GGAAS) resulted in dose-dependent inhibition of the 2N5.1 cell response to C14nef5 (Fig. 6B and C, respectively). Therefore, the C-terminal serine residue played a critical role in the activation of 2N5.1 cells and likely mediated an anchoring function. Furthermore, we found that excess amounts of the 5-mer peptide with a short acyl chain (C6-GGAIS) failed to block the response of 2N5.1 and SN45 T cells to C14nef5 (Fig. 6D and data not shown). Taken together, these results, obtained from inhibition experiments with an array of blockers, indicated that, whereas the attached myristic acid was important for the activation of both T cell lines, the C-terminal serine residue played a different role.

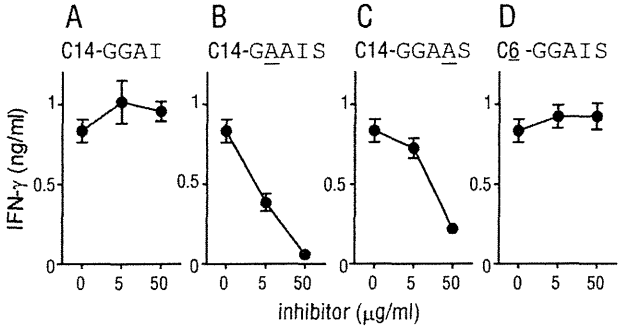


FIG 6 Inhibition of the response of 2N5.1 to C14nef5 by competitors. Irradiated autologous PBMCs were preincubated with excess amounts of the indicated blockers, for which mutated residues are underlined, and then the 2N5.1 responder cells and the C14nef5 Ag were added to the culture as described in Materials and Methods. After 24 h, the culture supernatants were collected, and the amount of IFN-γ released into the medium was measured. The error bars indicate SD.

## DISCUSSION

The analysis of the two $CD8^+$ T cell lines, 2N5.1 and SN45, that recognized the same lipopeptide Ag, C14nef5, revealed their shared and unshared properties, allowing us to grasp the molecular basis for lipopeptide Ag presentation and T cell activation (Fig. 7). One of the most remarkable similarities is that the optimal length of the attached acyl chain is $C_{14}$ (Fig. 5C). Both T cell lines failed to recognize Ags with a longer saturated acyl chain (C18nef5 and C22nef5), suggesting that the putative Ag-presenting molecules, tentatively termed LP1 for 2N5.1 and LP2 for SN45, may form a hydrophobic pocket with a depth suitable for accommodating the attached myristic acid. It should also be noted that the Ag with a $C_{10}$ acyl chain (C10nef5) was able to stimulate 2N5.1, but not SN45 (Fig. 5C), pointing to the possibility that the reduced hydrophobic interaction of the short acyl chain with the LP1 Ag-presenting molecules might be compensated for by an additional interaction, such as that mediated by an anchoring amino acid residue of the peptide, as discussed below. Such additional modes

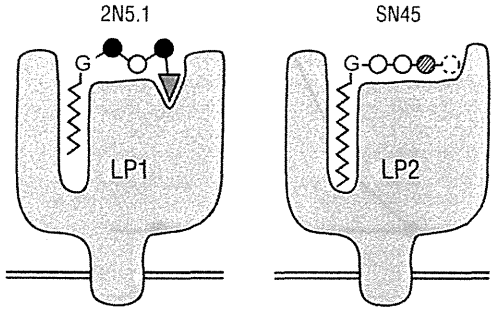


FIG 7 Schematic model of the putative Ag-presenting molecules for 2N5.1 (LP1) and SN45 (LP2). LP1 (left) has two separate Ag-binding sites, one for the acyl chain and the other for the anchoring serine residue (triangle) of C14nef5. The second (glycine) and fourth (isoleucine) residues (solid circles) are positioned outward for preferential interaction with the 2N5.1 TCR. Note that even the Nef 5-mer peptide with a saturated $C_{10}$ acyl chain (C10nef5) can bind to LP1 for recognition by 2N5.1, although its affinity for LP1 is lower than that of C14nef5. LP2 (right) also has an acyl-chain-binding pocket, but the serine residue critical for binding to LP1 is dispensable while the isoleucine residue (dashed circle) is essential. The myristic acid only fits into the hydrophobic pocket of LP2, and Ags with a longer or shorter acyl chain fail to be presented to the SN45 cells.

of interaction may be absent or only weak for LP2, resulting in a failure of SN45 to recognize C10nef5.

The present study also detected substantial differences in Ag recognition between the two cell lines. The C-terminal serine residue of C14nef5, a crucial element for the N-myristoylation motif (6), was an absolute requirement for recognition by 2N5.1, as the T cell line recognized C14nef5, but not C14nef4 with a C-terminal serine deletion (Fig. 5A). The excess amount of C14nef4 failed to inhibit the 2N5.1 reactivity to C14nef5, favoring the idea that this residue functions as an anchor for the stable binding of LP1 (Fig. 7, left, triangle). As discussed above, this interaction may play a significant role in capturing C10nef5, which has only weak affinity for the acyl-chain-accommodating pocket. Furthermore, the mutants with alanine substitutions (underlined) ($C_{14}$-G<u>A</u>AIS and $C_{14}$-GGA<u>A</u>S) were not recognized by 2N5.1 but were able to inhibit its recognition of C14nef5, indicating that the mutants indeed bound to LP1. Therefore, it would be reasonable to predict that the second glycine and the isoleucine residues (Fig. 7, left, solid circles) would be positioned preferentially for T cell recognition.

The putative Ag-presenting molecule, LP2, which mediates Ag presentation to SN45, appears much less stringent in terms of Ag binding. The C14nef4 Ag lacking the C-terminal serine residue could be recognized by SN45 as efficiently as or even more efficiently than C14nef5 (Fig. 5A), immediately excluding the anchoring model proposed for LP1 (Fig. 7, right, dashed circle). As C14nef3 failed to stimulate SN45, the fourth amino acid residue, isoleucine, would be particularly important for either binding to LP2, T cell recognition, or both. As described above, Ag binding to LP2 is likely to depend heavily on the full range of $C_{14}$ acyl chain interactions with the hydrophobic pocket.

Our study indicates that the T cell Ag repertoire of N-myristoylated peptides includes those with 4-mer and 5-mer peptides. Typically, N-myristoylation occurs for proteins with the N-terminal motif Gly-X-X-X-Ser/Thr (in which X is any amino acid) (6), and thus, the Ag diversity that can be generated as a result of amino acid alterations would be greatly limited compared with the 8- to 10-mer peptides presented by polymorphic MHC class I molecules. This indicates that, although introducing amino acid mutations in the target proteins is an efficient strategy that pathogenic viruses, such as HIV, have evolved to escape from cytotoxic T cell attack, the short stretch of the N-terminal amino acid residues of the Nef protein that contains N-myristoylation signal is hard to mutate without affecting the function of the protein. This also points to the possibility that the discrimination of foreign lipopeptides from self by the immune system may not be safely and strictly enforced. Viral infections are often associated with or followed by manifestations of autoimmune disorders (14–18), which could possibly be accounted for by the development of viral lipopeptide-specific T cells that may cross-react with self lipopeptides. On the other hand, products of a fraction of oncogenes, such as c-src, are N-myristoylated to function, and previous studies detected highly upregulated expression of *N*-myristoyl-transferase in cancer cells (19–22). Therefore, the aberrant or dysregulated expression of N-myristoylated cancer-associated proteins may result in activation of lipopeptide-specific T cells capable of recognizing abnormal cells derived from the self. The present study can potentially shed light on a new aspect of viral immunity, cancer immunity, and autoimmunity that has never been appreciated previously.

## ACKNOWLEDGMENTS

We thank Mariko Horiike for assistance in performing this study.

This work was supported by grants from the Japan Society for the Promotion of Science (grant numbers 22659188 and 24659481) and from the Senshin Medical Research Foundation (to M.S.). It was also supported by the Cooperation Research Program of the Primate Research Institute, Kyoto University. D.M. is a Research Fellow of the Japan Society for the Promotion of Science.

## REFERENCES

1. **Germain RN, Margulies DH.** 1993. The biochemistry and cell biology of antigen processing and presentation. Annu. Rev. Immunol. 11:403–450.
2. **Kasmar AG, van Rhijn I, Cheng TY, Turner M, Seshadri C, Schiefner A, Kalathur RC, Annand JW, de Jong A, Shires J, Leon L, Brenner M, Wilson IA, Altman JD, Moody DB.** 2011. CD1b tetramers bind alpha-beta T cell receptors to identify a mycobacterial glycolipid-reactive T cell repertoire in humans. J. Exp. Med. 208:1741–1747.
3. **Komori T, Nakamura T, Matsunaga I, Morita D, Hattori Y, Kuwata H, Fujiwara N, Hiromatsu K, Harashima H, Sugita M.** 2011. A microbial glycolipid functions as a new class of target antigen for delayed-type hypersensitivity. J. Biol. Chem. 286:16800–16806.
4. **Dascher CC, Hiromatsu K, Xiong X, Morehouse C, Watts G, Liu G, McMurray DN, LeClair KP, Porcelli SA, Brenner MB.** 2003. Immunization with a mycobacterial lipid vaccine improves pulmonary pathology in the guinea pig model of tuberculosis. Int. Immunol. 15:915–925.
5. **Moody DB, Ulrichs T, Muhlecker W, Young DC, Gurcha SS, Grant E, Rosat JP, Brenner MB, Costello CE, Besra GS, Porcelli SA.** 2000. CD1c-mediated T-cell recognition of isoprenoid glycolipids in Mycobacterium tuberculosis infection. Nature 404:884–888.
6. **Boutin JA.** 1997. Myristoylation. Cell Signal. 9:15–35.
7. **Aldrovandi GM, Gao L, Bristol G, Zack JA.** 1998. Regions of human immunodeficiency virus type 1 nef required for function in vivo. J. Virol. 72:7032–7039.
8. **Morita D, Igarashi T, Horiike M, Mori N, Sugita M.** 2011. Cutting edge: T cells monitor N-myristoylation of the Nef protein in simian immunodeficiency virus-infected monkeys. J. Immunol. 187:608–612.
9. **Morita D, Katoh K, Harada T, Nakagawa Y, Matsunaga I, Miura T, Adachi A, Igarashi T, Sugita M.** 2008. Trans-species activation of human T cells by rhesus macaque CD1b molecules. Biochem. Biophys. Res. Commun. 377:889–893.
10. **DerSimonian H, Sugita M, Glass DN, Maier AL, Weinblatt ME, Reme T, Brenner MB.** 1993. Clonal V alpha 12.1+ T cell expansions in the

peripheral blood of rheumatoid arthritis patients. J. Exp. Med. 177:1623–1631.
11. **Uematsu Y, Wege H, Straus A, Ott M, Bannwarth W, Lanchbury J, Panayi G, Steinmetz M.** 1991. The T-cell-receptor repertoire in the synovial fluid of a patient with rheumatoid arthritis is polyclonal. Proc. Natl. Acad. Sci. U. S. A. **88**:8534–8538.
12. **Kestler HW III, Li Y, Naidu YM, Butler CV, Ochs MF, Jaenel G, King NW, Daniel MD, Desrosiers RC.** 1988. Comparison of simian immunodeficiency virus isolates. Nature **331**:619–622.
13. **Matsuda JL, Gapin L, Sidobre S, Kieper WC, Tan JT, Ceredig R, Surh CD, Kronenberg M.** 2002. Homeostasis of V alpha 14i NKT cells. Nat. Immunol. **3**:966–974.
14. **Fitzpatrick EA, Avdiushko M, Kaplan AM, Cohen DA.** 1999. Role of virus replication in a murine model of AIDS-associated interstitial pneumonitis. Exp. Lung Res. **25**:647–661.
15. **Kang JA, Mohindru M, Kang BS, Park SH, Kim BS.** 2000. Clonal expansion of infiltrating T cells in the spinal cords of SJL/J mice infected with Theiler's virus. J. Immunol. **165**:583–590.
16. **Mokhtarian F, Shi Y, Zhu PF, Grob D.** 1994. Immune responses, and autoimmune outcome, during virus infection of the central nervous system. Cell. Immunol. **157**:195–210.
17. **Ohyama Y, Carroll VA, Deshmukh U, Gaskin F, Brown MG, Fu SM.** 2006. Severe focal sialadenitis and dacryoadenitis in NZM2328 mice induced by MCMV: a novel model for human Sjogren's syndrome. J. Immunol. **177**:7391–7397.
18. **Watanabe R, Wege H, ter Meulen V.** 1983. Adoptive transfer of EAE-like lesions from rats with coronavirus-induced demyelinating encephalomyelitis. Nature **305**:150–153.
19. **Boutin JA, Ferry G, Ernould AP, Maes P, Remond G, Vincent M.** 1993. Myristoyl-CoA:protein N-myristoyltransferase activity in cancer cells. Purification and characterization of a cytosolic isoform from the murine leukemia cell line L1210. Eur. J. Biochem. **214**:853–867.
20. **Patwardhan P, Resh MD.** 2010. Myristoylation and membrane binding regulate c-Src stability and kinase activity. Mol. Cell. Biol. **30**:4094–4107.
21. **Rajala RV, Datla RS, Moyana TN, Kakkar R, Carlsen SA, Sharma RK.** 2000. N-myristoyltransferase. Mol. Cell. Biochem. **204**:135–155.
22. **Shoji S, Kurosawa T, Inoue H, Funakoshi T, Kubota Y.** 1990. Human cellular src gene product: identification of the myristoylated pp60c-src and blockage of its myristoyl acylation with N-fatty acyl compounds resulted in the suppression of colony formation. Biochem. Biophys. Res. Commun. **173**:894–901.
23. **Grant EP, Degano M, Rosat JP, Stenger S, Modlin RL, Wilson IA, Porcelli SA, Brenner MB.** 1999. Molecular recognition of lipid antigens by T cell receptors. J. Exp. Med. **189**:195–205.
24. **Manning CH, Heise ER.** 1991. Biochemical analysis of class I and class II MHC antigens in cynomolgus macaques by one-dimensional isoelectric focusing. Tissue Antigens **37**:56–65.
25. **Parham P, Ploegh HL.** 1980. Molecular characterization of HLA-A, B homologues in owl monkeys and other nonhuman primates. Immunogenetics **11**:131–143.
26. **Sugita M, Kumagai S, Ota M, Inoko H, Tsuji K, Imura H.** 1992. Demonstration of the requirement for self antigen in the activation of autoreactive T cells. Int. Immunol. **4**:119–124.

Virology 436 (2013) 100–111

Contents lists available at SciVerse ScienceDirect

Virology

journal homepage: www.elsevier.com/locate/yviro

# Generation of a replication-competent chimeric simian-human immunodeficiency virus carrying *env* from subtype C clinical isolate through intracellular homologous recombination

Yasuhisa Fujita, Hiroyuki Otsuki, Yuji Watanabe, Mika Yasui, Takeshi Kobayashi, Tomoyuki Miura*, Tatsuhiko Igarashi**

*Laboratory of Primate Model, Experimental Research Center for Infectious Diseases, Institute for Virus Research, Kyoto University, Kyoto 606-8507, Japan*

ARTICLE INFO

*Article history:*
Received 19 August 2012
Returned to author for revisions
10 September 2012
Accepted 29 October 2012
Available online 6 December 2012

*Keywords:*
Intracellular homologous recombination
Simian-human immunodeficiency virus
Clinical isolate
Subtype C
CCR5-tropism
*In vitro* passage
Alveolar macrophage
*In vivo* passage
Animal model
AIDS

ABSTRACT

A new simian-human immunodeficiency virus (SHIV), carrying *env* from an uncloned HIV-1 subtype C clinical isolate (97ZA012), was generated through intracellular homologous recombination, a DNA repair mechanism of the host cell. PCR fragments amplified from an existing SHIV plasmid (a 7-kb fragment from the 5′ end and a 1.5-kb fragment from the 3′ end) and a 4-kb fragment amplified from 97ZA012 cDNA containing *env* were co-transfected to human lymphoid cells. The resulting recombinant was subjected to serial passage in rhesus peripheral blood mononuclear cells (RhPBMCs). The resulting SHIV 97ZA012 was replication competent in RhPBMCs and monkey alveolar macrophages, and possessed CCR5 preference as an entry co-receptor. Experimental infection of rhesus macaques with SHIV 97ZA012 caused high titers of plasma viremia and a transient but profound depletion of $CD4^+$ T lymphocytes in the lung. Animal-to-animal passage was shown to be a promising measure for further adaptation of the virus in monkeys.



## Introduction

Human immunodeficiency virus (HIV) infections have been a major global public health issue since their initial recognition in the 1980s. Globally, approximately 33 million individuals are living with HIV, 1.8 million people die of HIV-related complications, and 2.6 million people newly acquired the virus in 2009 (UNAIDS, 2010). Establishment of effective preventive measures is urgently needed to control the epidemic.

Extensive genomic diversity is a characteristic trait of HIV. HIV type 1 (HIV-1), the major genotype of the virus, comprises four subgroups: M, N, O, and P. Subgroup M further comprises numerous subtypes and circulating recombinant forms (CRFs), which are recombinant viruses among subtypes. Among the subtypes, subtype C plays a leading role in the epidemic, accounting for nearly 50% of global HIV infections (Hemelaar et al., 2011). Greater numbers of viral particles are detected in the vaginal secretions of pregnant individuals infected with subtype C than from persons infected with subtypes A or D (John-Stewart et al., 2005), potentially making subtype C more transmissible than others and rendering it predominant in the current epidemic. A compact V1/V2 loop and threonine at 316 located in the V3 loop of Env, distinct features shared by many subtype C isolates, may contribute to preferential replication of these viruses in the genital tract (Walter et al., 2009).

The humoral immune reaction directed against subtype C virus is unequal to that directed against subtype B virus. Virus-neutralizing antibodies mounted in individuals infected with subtype C are directed against the alpha-2 helix in the Env C3 region. This region is rarely immunogenic in subtype B virus infection (Moore et al., 2008), indicating a conformational difference in Env between these subtypes. The development of a tractable animal model for subtype C is thus necessary to establish a strategy for effective induction of neutralizing antibodies directed against the protein of this particular subtype.

* Corresponding author at: Room 303, Molecular Biology Research Bldg., Institute for Virus Research, Kyoto University, 53 Kawahara-cho, Shogoin, Sakyo ward, Kyoto, Kyoto 606-8507, Japan. Fax: +81 75 761 9335.
** Corresponding author at: Room 301, Molecular Biology Research Bldg., Institute for Virus Research, Kyoto University, 53 Kawahara-cho, Shogoin, Sakyo ward, Kyoto, Kyoto 606-8507, Japan. Fax: +81 75 761 9335.
*E-mail addresses:* tmiura@virus.kyoto-u.ac.jp (T. Miura), tigarash@virus.kyoto-u.ac.jp (T. Igarashi).

0042-6822/$ - see front matter © 2012 Elsevier Inc. All rights reserved.
http://dx.doi.org/10.1016/j.virol.2012.10.036

Simian-human immunodeficiency virus (SHIV) carrying Env derived from subtype C would be an especially vital tool because it would allow for evaluation of the effectiveness of vaccine-induced immunity in the context of virus infection *in vivo*.

However, only a few subtype C SHIVs are available, and none reproducibly replicates to high titers and induces disease in monkeys. In addition, limited numbers of SHIVs utilize the CCR5 molecule as an entry co-receptor. The scarcity of available SHIV strains is attributed to the difficulty in generating an infectious chimeric virus. SHIVs have been generated through recombinant DNA techniques involving implantation of a chunk of genes, such as *tat*, *rev*, *vpu*, and *env*, from the molecular clone of parental HIV-1 into the backbone of the SIV239 molecular clone. This method does not always lead to successful generation of infectious SHIV. Two presumable reasons may explain this difficulty: (1) incompatibility of a particular clone from the parental HIV-1 swarm with the SIV backbone and (2) inadequate employment of "breakpoints," sites of recombination, for the given parental clones of HIV-1 and SIV. The generation of SHIVs by the conventional technique (*i.e.*, recombination of HIV-1 genes from a molecular clone verified to be infectious to human cells with an SIV backbone at breakpoints that are reasonably assumed to be appropriate) may represent a major bottleneck for the development of new SHIV strains.

Intracellular homologous recombination (IHR) is a cellular mechanism for the restoration of DNA double-strand breaks. It also takes place when exogenously introduced DNA fragments share "homologous sequences" (Srinivasan et al., 1989). The mechanism has been attributed to the generation of infectious HIV-1 particles from cell lines carrying multiple defective provirus genomes (Inoue et al., 1991). IHR also causes generation of infectious HIV-1 through co-transfection of truncated viral cDNA clones into the cells (Kalyanaraman et al., 1988; Srinivasan et al., 1989) or through recombination between exogenous sequences and integrated chromosomal HIV sequences (Clavel et al., 1989; Srinivasan et al., 1989). It is then utilized as a measure to readily generate recombinant HIV-1 (Cheng-Mayer et al., 1990; Hertogs et al., 1998; Kellam and Larder, 1994).

We reasoned that generation of SHIV through IHR could circumnavigate the above-mentioned issues and accelerate the process as follows: (1) DNA fragments prepared by polymerase chain reaction (PCR) with cDNA from an uncloned HIV-1 genome would provide a continuum of heterogeneous sequences that potentially contain competent clone(s) in the context of infection in monkey cells *in vitro* and monkeys *in vivo* when combined with an SIV backbone, and (2) random occurrence of IHR within "homologous sequences" would likely produce multiple SHIV genomes with breakpoints at various sites, increasing the chance for emergence of a virus with favorable fitness. In addition, co-transfection of DNA fragments into cells susceptible to viral infection would subject the generated recombinant virus to multi-round replication, causing selection/evolution of a replication-competent virus. Based on this reasoning, we embarked on IHR-mediated generation of SHIV to investigate the utility of these potential advantages.

## Results

### *Generation of recombinant virus through IHR*

To generate a novel SHIV carrying the *env* gene derived from a clinical isolate of subtype C HIV-1 through IHR, we prepared three DNA fragments by PCR as depicted in Fig. 1. Approximately 1100 bps of overlapping sequence (where IHR was expected to take place) were shared by Fragments I and III, 1400 bps were shared by Fragments II-a and III, and 1200 bps were shared by Fragments II-b and III (Fig. 1).

Although we envisioned that recombination between the two DNA fragments could theoretically take place at any base within these overlaps, potentially resulting in generation of multiple sets of recombinant genomes, only replication-competent recombinant(s) would emerge as representative following transfection with these fragments into susceptible cells for lentiviral replication and multi-round replication cycles. To test this hypothesis, mixtures of Fragments I, II-a, and III (Transfection #1) or Fragments I, II-b, and III (Transfection #2), 0.2 μg of each DNA preparation, were co-transfected to human T-lymphoid cell line C8166-CCR5 cells. The cultures were maintained for 3 weeks to monitor emergence of recombinant virus by microscopic observation because the parental HIV-1 97ZA012, which contributed the *env* gene to the transfection, was known to induce syncytia in the cells (data not shown). Transfection #1 produced syncytia on day

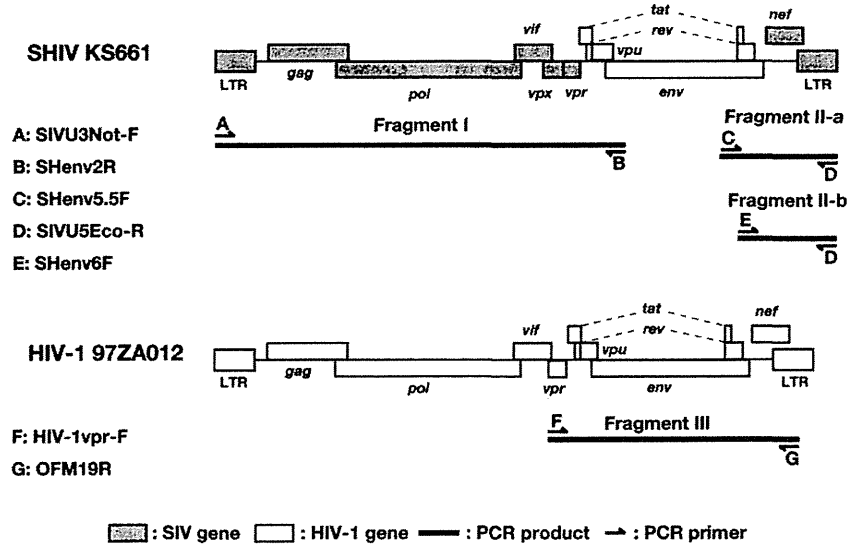


**Fig. 1.** Schematic representation of HIV-1/SHIV genome organizations and PCR fragments employed for co-transfection. Filled boxes represent genes derived from SIV. Open boxes represent genes derived from HIV-1. SHIV KS661, existing SHIV, carries *tat*, *rev*, *vpu*, and *env* genes from subtype B HIV-1 89.6. Broad lines represent PCR fragments; Fragments I and II-a/II-b were amplified using plasmid DNA of SHIV KS661 as a template. Fragment III was amplified from cDNA of the HIV-1 97ZA012 genome as a template. Arrows represent PCR primers whose identifiers are depicted in the figure.

14 post-transfection, and Transfection #2 caused syncytia on day 15. A small portion of each culture was collected on the day of syncytia emergence and co-cultivated with uninfected C8166-CCR5 cells to determine whether the syncytia would spread. Both initiated robust syncytia formation within 24 h post co-cultivation, suggesting generation of a recombinant virus capable of replicating in C8166-CCR5 cells. Culture supernatants collected at 3 days post-co-culture, *viz.* 17 days post-Transfection #1 and 18 days post-Transfection #2, were combined and used as starting material for *in vitro* selection/adaptation.

*In vitro passage of the recombinant virus*

Because we aimed to generate a new SHIV strain to be used in a macaque model, which requires a virus with the capacity to replicate to a high titer, we first subjected the "syncytium-inducing agent," which emerged through IHR, to sequential passage in rhesus macaque PBMCs (RhPBMC). We envisioned that a certain population of the recombinant carrying a suitable genotype from the parental virus swarm and appropriate recombination breakpoints might outgrow and/or evolve through the passage. Newly generated recombinant viruses are known in general to be less replication competent, especially in RhPBMCs. Such viruses have replicated better when inoculated into $CD4^+$ cell-enriched RhPBMCs by deletion of $CD8^+$ cells (Chen et al., 2000; Kamada et al., 2006). Although the viral agent was robustly replicating in human C8166-CCR5 cells, we followed the previous observations and inoculated 100 μl filtered culture supernatant of the cells into $2 \times 10^6$ rhesus macaque $CD4^+$ cell-enriched RhPBMCs (Passage #1). Virus replication was monitored by virion-associated reverse transcriptase (RT) activity released in the culture supernatant (Fig. 2).

Passage #1 revealed that the virus indeed replicated in $CD4^+$ cell-enriched RhPBMCs (Fig. 2A). The virus replicated to an initial peak of RT activity on day 3 with 2000 cpm/μl supernatant equivalent, and replication was then reduced somewhat on day 4 (1250 cpm), likely because of the addition of fresh $CD4^+$ cell-enriched PBMCs. Replication increased again to 2170 cpm on day 5, the highest RT activity in this passage. The RT activity was maintained at a high level during the subsequent 2 days (1900–2000 cpm), then declined rapidly on day 8. Cryopreserved culture supernatant (50 μl) collected from day 5 of Passage #1 was inoculated to $2 \times 10^6$ newly prepared $CD4^+$ cell-enriched RhPBMCs to confirm the observed replication property of the virus (Passage #2). Although replication in Passage #2 took longer than that in Passage #1, the Passage #2 virus also replicated to a high titer, 2180 cpm/μl supernatant equivalent on day 8, followed by a sharp decline on day 9 (1250 cpm; Fig. 2B).

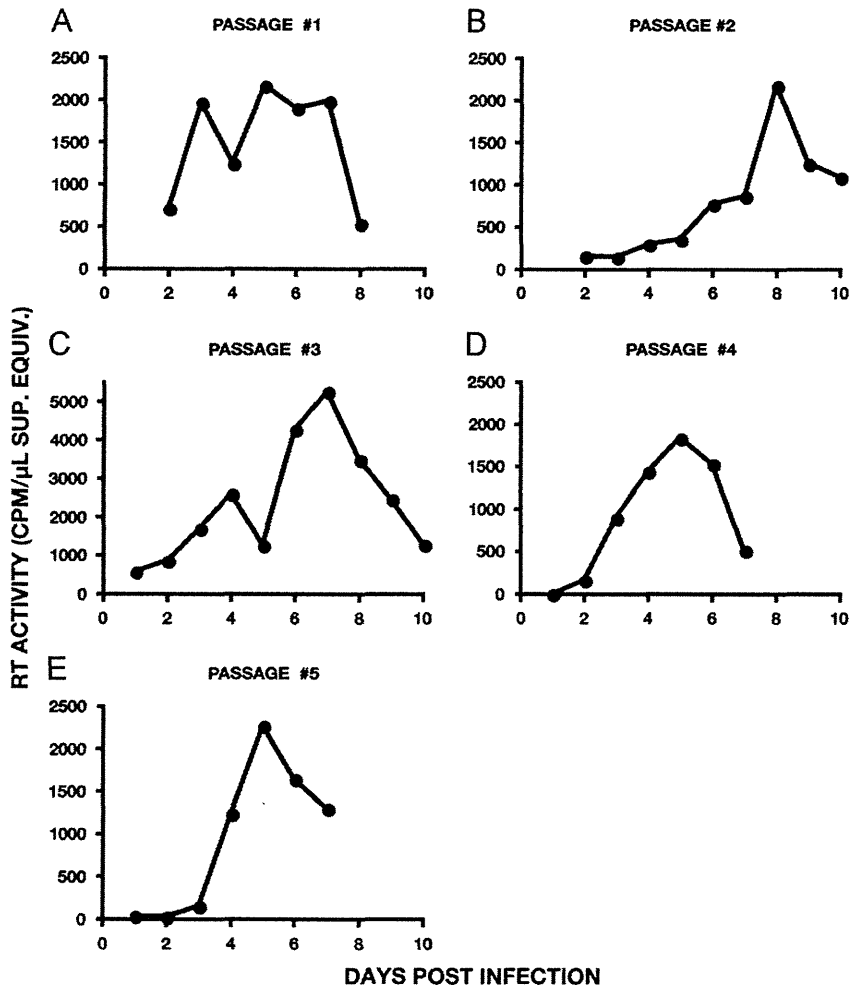


**Fig. 2.** Passage of the recombinant virus through RhPBMCs. Recombinant virus that emerged from C8166-CCR5 cells co-transfected with PCR fragments was serially passed through RhPBMCs (A–E). A small amount of supernatant was collected from each culture daily, and virion-associated reverse transcriptase (RT) activity was assessed. RT activities were represented as radioactive counts per minute (cpm) induced by 1 μl culture supernatant equivalent. $CD4^+$ cell-enriched RhPBMCs were employed for Passages #1–3 (A–C), and whole RhPBMCs were utilized for Passages #4 and #5 (D and E). Filtered culture supernatant was used to pass virus from existing culture to new culture, except from Passage #2 to #3, in which the mixture of cells and supernatant was inoculated to freshly prepared cells.

Because the virus appeared to reproducibly replicate in CD4$^+$ cell-enriched RhPBMCs, we next examined whether the virus could replicate in unmanipulated RhPBMCs, a cell preparation without enrichment of CD4$^+$ cells, by taking a small portion of the ongoing culture on day 8 and co-cultivating it with fresh whole RhPBMCs (Passage #3). For this experiment, we monitored the RT activity of the culture supernatant from Passage #2 daily and decided to set up Passage #3 because of a substantial increase in RT activity on day 8. Passage #3 resulted in robust virus replication that reached 5,250 cpm/μl supernatant equivalent on day 7, then declined during the following days, suggesting that it possessed replication capacity in unmanipulated RhPBMCs (Fig. 2C). To determine whether we could reproduce this observation in a more rigorous setting, culture supernatant without cells, collected on day 7 from Passage #3, was inoculated into whole RhPBMCs newly prepared from normal rhesus macaques (Passage #4). The virus replicated robustly to a high titer, reaching 1850 cpm/μl supernatant equivalent on day 5, followed by a rapid decline (Fig. 2D). To confirm the observation, we inoculated supernatant collected on day 5 of Passage #4 into another RhPBMC preparation without manipulation a second time (Passage #5). The virus reproducibly replicated in primary monkey cells, with a peak of RT activity on day 5 post-infection (2280 cpm; Fig. 2E). We concluded that a new recombinant virus capable of replicating in RhPBMCs was generated/evolved through IHR/*in vitro* passage. We designated the culture supernatant collected on day 5 from Passage #5 as SHIV 97ZA012 and subjected it to further characterization.

*Genomic organization of SHIV 97ZA012*

To elucidate the genomic organization of SHIV 97ZA012, the nt sequence was determined on cDNA that was reverse-transcribed from virion-associated viral genomic RNA prepared from the culture supernatant. The obtained sequence was compared with those of SHIV KS661 and HIV-1 97ZA012 (Fig. 3). Genomic analysis revealed that the 5′ and 3′ breakpoints were at the 282nd nt of *env* gp120, upstream of the V1/V2 loop, and the 756th nt of the *env* gp41 cytoplasmic domain, respectively (Fig. 3A). The breakpoints that gave rise to replication-competent virus were not necessarily at the interface of genes juxtaposed to each other. This is also the case in many CRFs of HIV-1, examples of naturally occurring recombinants (Carr et al., 2001; Guimaraes et al., 2008; Koulinska et al., 2001; Perez et al., 2006; Piyasirisilp et al., 2000).

SimPlot (Lole et al., 1999) analysis revealed that the genomic fragment derived from HIV-1 97ZA012 did not completely match

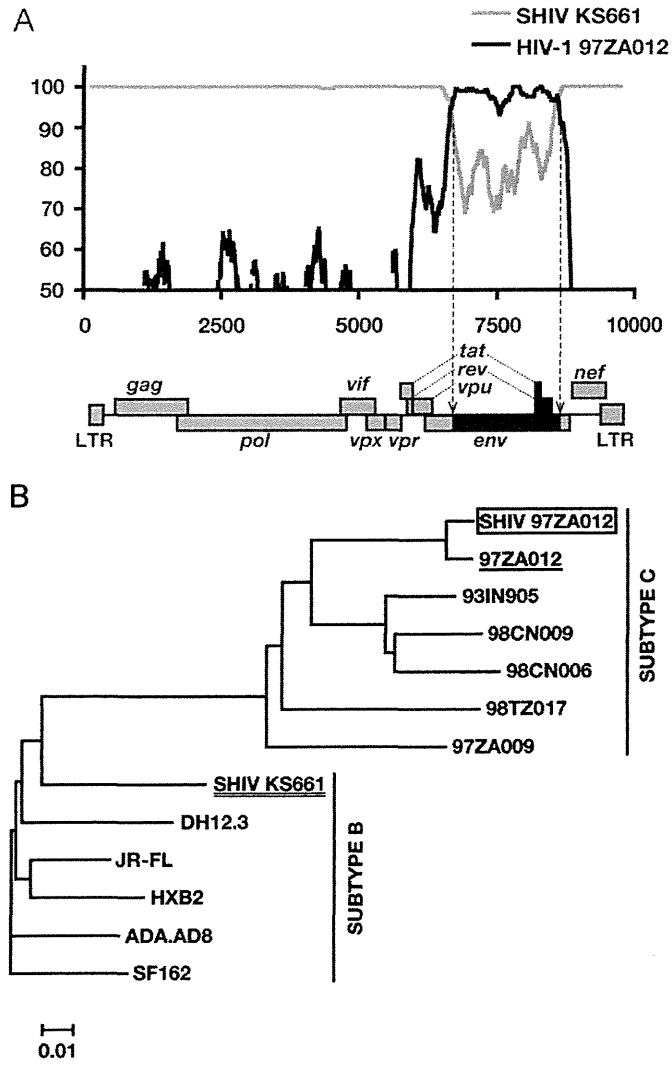


**Fig. 3.** Genomic organization of SHIV 97ZA012. (A) Breakpoints in SHIV 97ZA012 were analyzed by the SimPlot program with SHIV KS661 (gray) and HIV-1 97ZA012 (black) as references. Schematic SHIV genome organization was aligned to similarity plot for a visual purpose. (B) Phylogenetic analysis of SHIV 97ZA012 *env* portion. The gene portion identified in (A), between nt 6429 and 8325 (in HIV-1 HXB2) and derived from HIV-1 97ZA012, was subjected to phylogenetic analysis with the corresponding sequence of the reference virus isolates. The phylogenetic tree was generated by the neighbor-joining method.

the registered sequence of the virus (GenBank Accession No. AF286227). To ascertain that the recombinant virus indeed carries the *env* sequence derived from HIV-1 97ZA012, we conducted a phylogenetic analysis of the sequence with the corresponding region of HIV-1 strains belonging to subtype B or C, including the registered sequence of 97ZA012 (Fig. 3B). The supposed 97ZA012-derived sequence naturally formed a subcluster with the registered sequence and was positioned in the cluster of subtype C strains in the phylogenetic tree. We concluded that the observed difference in sequences between SHIV 97ZA012 and the registered HIV-1 97ZA012 was within the extent of quasispecies of a single isolate.

### *Replication properties of SHIV 97ZA012 in C8166-CCR5 cells and RhPBMCs*

To characterize the replication properties of SHIV 97ZA012, we inoculated the virus into human C8166-CCR5 cells and RhPBMCs. Because HIV-1 is unable to replicate in monkey cells, the relative replication capability of the newly generated virus to the parental HIV-1 97ZA012 was assessed in C8166-CCR5 cells. SHIV KS661, which provided the backbone for SHIV 97ZA012, was also examined. In RhPBMCs, replication of SHIV 97ZA012 was compared with that of SIV239, the most widely used SIV. The viruses were normalized to an infectious unit (multiplicity of infection [MOI]=0.01 or 0.1 median tissue culture infective dose [$TCID_{50}$/cell]) and inoculated into these cells. Replication of the viruses was monitored by virion-associated RT activity in the culture supernatant (Fig. 4). Because C8166-CCR5 cells were highly susceptible to HIV-1/SIV and progressed to cell death, infections at a higher multiplicity (MOI=0.1) resulted in lower peak RT activities compared with those at a lower multiplicity (Fig. 4A). Regardless of multiplicity, SHIV 97ZA012 exhibited a slower replication kinetic compared with that of the parental HIV-1 97ZA012, likely due to the chimeric structure of the virus (Li et al., 1992; Shibata et al., 1991) or to the result of adaptation to monkey cells. SHIV KS661 also exhibited faster replication kinetics compared with SHIV 97ZA012.

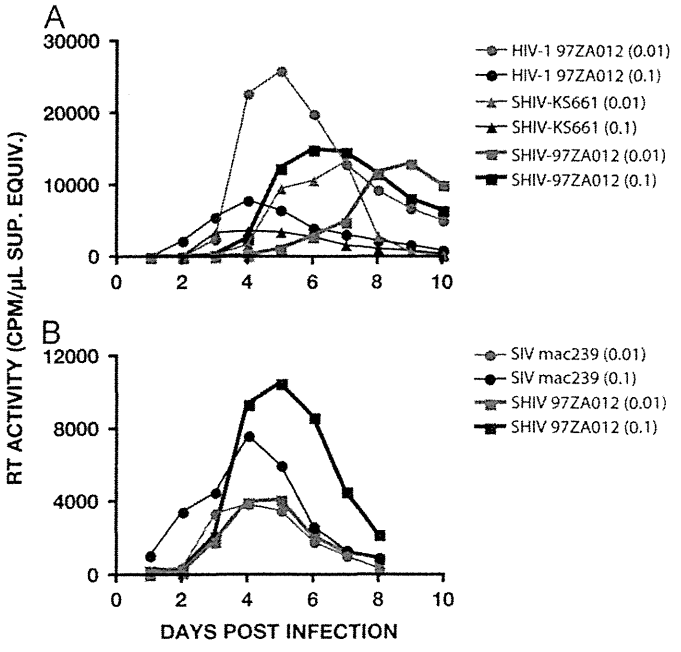


**Fig. 4.** Replication of SHIV 97ZA012 in C8166-CCR5 cells (A) and RhPBMCs (B). The replication property of SHIV 97ZA012 in these cells was compared with those of HIV-1 97ZA012, SHIV KS661 (A) and SIV239 (B). The viruses were normalized by the infectious unit (MOI=0.01 and 0. 1 TCID50/cell) and spinoculated to these cells at 1200 × *g* for 60 min. Gray symbols/lines represent virus replication at MOI=0.01, and black symbols/lines represent virus replication at MOI.=0.1. Culture supernatant was collected daily, and virion-associated reverse transcriptase activities were assessed.

While SHIV 97ZA012 exhibited a slower replication profile compared with the reference viruses in C8166-CCR5 cells, replication of SHIV 97ZA012 in RhPBMCs was comparable with that of SIV239 (Fig. 4B). Infection at a MOI=0.01 resulted in somewhat more production of progeny in SIV239 than in SHIV 97ZA012 during the first 3 days. When the experiment was set up at a MOI=0.1, SIV239 produced markedly more progeny than did SHIV 97ZA012 during the first 3 days of infection, while SHIV 97ZA012 replicated to higher titers than did SIV239 at day 4 and thereafter. To estimate the total production of progeny virus during the observation period, the areas under the curve (AUC) of each virus were compared. The AUC of SHIV 97ZA012 was approximately 1.5-fold greater than that of SIV (data not shown). Based on these data, we concluded that SHIV 97ZA012 is as replication competent as SIV239 in rhesus macaque PBMCs.

### *Co-receptor preference of SHIV 97ZA012*

The parental HIV-1 97ZA012 strain reportedly utilizes CCR5 as an entry co-receptor (Broder and Jones-Trower, 1999). The chimeric structure of gp120 carried by SHIV 97ZA012 (between KS661, which was originally derived from HIV-1 89.6, and 97ZA012) and uncertainty of the co-receptor preference of 97ZA012 Env in the context of the SHIV/macaque cell system prompted us to subject SHIV 97ZA012, along with control viruses, to a co-receptor usage assay. Each virus, normalized by an infectious unit, was inoculated to RhPBMCs in the presence of 5 μM AMD3100 (a small-molecule CXCR4 inhibitor), AD101 (a small-molecule CCR5 inhibitor), or both. Virus replication was monitored for 7 days by virion-associated RT activity release in the culture supernatant (Fig. 5). SIV239, which has been established as a CCR5-utilizing virus, replicated to a high titer in the absence of any inhibitor (Fig. 5A). AMD3100 had little impact on the replication of the virus, as described previously (Zhang et al., 2000). In the presence of AD101 or both inhibitors, however, replication of SIV239 was substantially impaired. In contrast, SHIV KS661, which has been reported to predominantly utilize CXCR4 as an entry co-receptor (Matsuda et al., 2010), exhibited a replication profile opposite to that of SIV239: no impairment of replication in the presence of AD101, but remarkably delayed replication in the presence of AMD3100, and complete suppression in the presence of both inhibitors (Fig. 5B). When control viruses exhibited the replication profiles described above, SHIV 97ZA012 exhibited a replication profile similar to that of SIV239: no impact on replication in the presence of AMD3100, but complete suppression when AD101 was present in the culture (Fig. 5C). Based on these results, we concluded that SHIV 97ZA012 is a CCR5-utilizing virus, as is the parental HIV-1 97ZA012 in human cells.

### *Replication of SHIV 97ZA012 in macrophages*

Many CCR5-utilizing HIV-1 strains replicate in monocyte-derived macrophages, which is a biological property called "macrophage tropism." Macrophage tropism has been shown to be associated with viral neurotropism (Gorry et al., 2001), a subject to be investigated in non-human primate AIDS models. To clarify the biological property of the virus in macrophages, SHIV 97ZA012, along with macrophage-tropic and non-macrophage-tropic viruses, normalized by RT activity was inoculated to rhesus macaque primary alveolar macrophage (RhAM) cultures prepared from three uninfected animals. Virus replication was monitored by virion-associated RT activity released in